Wireless-Powered Over-the-Air Computation in Intelligent Reflecting Surface-Aided IoT Networks

Zhibin Wang, *Student Member, IEEE*, Yuanming Shi, *Member, IEEE*, Yong Zhou, *Member, IEEE*, Haibo Zhou, *Senior Member, IEEE*, and Ning Zhang, *Senior Member, IEEE*

***Abstract*—Fast wireless data aggregation and efficient battery recharging are two critical design challenges of Internet-of-Things (IoT) networks. Over-the-air computation (AirComp) and energy beamforming (EB) turn out to be two promising techniques that can address these two challenges, necessitating the design of wireless-powered AirComp. However, due to severe channel propagation, the energy harvested by IoT devices may not be sufficient to support AirComp. In this article, we propose to leverage the intelligent reflecting surface (IRS) that is capable of dynamically reconfiguring the propagation environment to drastically enhance the efficiency of both downlink EB and uplink AirComp in IoT networks. Due to the coupled problems of downlink EB and uplink AirComp, we further propose the joint design of energy and aggregation beamformers at the access point, downlink/uplink phase-shift matrices at the IRS, and transmit power at the IoT devices, to minimize the mean-squared error (MSE), which quantifies the AirComp distortion. However, the formulated problem is a highly intractable nonconvex quadratic programming problem. To solve this problem, we first obtain the closed-form expressions of the energy beamformer and the device transmit power, and then develop an alternating optimization framework based on difference-of-convex programming to design the aggregation beamformers and IRS phase-shift matrices. Simulation results demonstrate the performance gains of the proposed algorithm over the baseline methods and show that deploying an IRS can significantly reduce the MSE of AirComp.**

***Index Terms*—Energy beamforming (EB), intelligent reflecting surface (IRS), Internet of Things (IoT), over-the-air computation (AirComp), wireless data aggregation (WDA).**

Manuscript received February 29, 2020; revised May 27, 2020; accepted July 29, 2020. Date of publication August 10, 2020; date of current version January 22, 2021. This work was supported by the National Natural Science Foundation of China (NSFC) under Grant 61971286. This article was presented in part at IEEE VTC Spring, Antwerp, Belgium, May 2020. *(Corresponding author: Yong Zhou.)*

Zhibin Wang is with the School of Information Science and Technology, ShanghaiTech University, Shanghai 201210, China, also with the Shanghai Institute of Microsystem and Information Technology, Chinese Academy of Sciences, Shanghai 200050, China, and also with the University of Chinese Academy of Sciences, Beijing 100049, China (e-mail: wangzhb@shanghaitech.edu.cn).

Yuanming Shi and Yong Zhou are with the School of Information Science and Technology, ShanghaiTech University, Shanghai 201210, China (e-mail: shiym@shanghaitech.edu.cn; zhouyong@shanghaitech.edu.cn).

Haibo Zhou is with the School of Electronic Science and Engineering, Nanjing University, Nanjing 210023, China (e-mail: haibozhou@nju.edu.cn).

Ning Zhang is with the Department of Electrical and Computer Engineering, University of Windsor, Windsor, ON N9B 3P4, Canada (e-mail: ning.zhang@uwindsor.ca).

Digital Object Identifier 10.1109/JIOT.2020.3015489

I. Introduction

With the advancement of wireless technologies, Internet of Things (IoT) is envisioned to provide ubiquitous connectivity for billions of physical devices (e.g., sensors, actuators, and smartphones) with sensing, processing, and communication capabilities to collect and share data with minimum human intervention [1]–[3]. Typical emerging IoT applications include environmental monitoring, smart home, healthcare, connected vehicles, and industrial automation. To unleash the full potential of IoT networks, the following two research challenges, among others, need to be addressed. First, due to the scarcity of the radio spectrum, fast wireless data aggregation (WDA) from a large number of distributed IoT devices is a critical design challenge for many latency-sensitive IoT applications (e.g., sensing results fusion and distributed consensus). Second, efficient powering for densely placed IoT devices is another research challenge in IoT networks, as the IoT devices are usually battery powered and their batteries are difficult to be replaced.

Over-the-air computation (AirComp) and wireless power transfer (WPT) are two promising technologies that can address each of the aforementioned challenges in IoT networks. Specifically, AirComp is capable of achieving fast WDA by reducing the transmission and computation latency [4]–[17]. By exploiting the waveform superposition property of multiaccess channels, AirComp merges the concurrent data transmission from multiple IoT devices and the nomographic function (e.g., averaging and geometric mean) computation. With concurrent transmission, AirComp achieves a low transmission latency that is independent of the number of IoT devices, thereby enabling fast WDA. On the other hand, WPT has the potential to alleviate the energy constraints of IoT devices by enabling them to harvest energy from the ambient radio-frequency (RF) radiation [18]–[20].

The integration of AirComp and energy beamforming (EB) in IoT networks was recently studied in [21], where the IoT devices utilized the harvested energy to support AirComp. However, due to severe channel propagation, the harvested energy may not be sufficient to support reliable uplink transmission, leading to high AirComp distortion. As a result, it is critical to mitigate the detrimental effects of channel fading, so as to further enhance the efficiency of both EB and AirComp in IoT networks. Fortunately, intelligent reflecting surface (IRS) has recently been recognized as a promising solution that can enhance the spectrum and energy efficiency of wireless networks by reconfiguring the wireless

propagation environments [22]–[24]. This motivates us to design wireless-powered AirComp in IRS-aided IoT networks.

A. Related Works

The research on AirComp has recently attracted considerable attention [4]–[17]. In particular, the seminal work [4] showed that the concurrent transmission of analog modulated signals facilitates fast functional computation in wireless sensor networks. Abari *et al.* [5] generalized the AirComp mechanism to compute various target functions. A simple analog AirComp scheme was proposed in [6] to achieve robust estimations of computing functions in wireless sensor networks. To compensate the nonuniform fading of different sensors, Chen *et al.* [7] proposed a uniform-forcing transceiver design to achieve reliable AirComp. Zhu and Huang [8] and Chen *et al.* [9] exploited the advantages of AirComp to achieve efficient multimodal sensing and multiple functions computation, respectively. Besides, a blind AirComp scheme was proposed in [10] for latency reduction in IoT networks without relying on the channel state information (CSI). As the principle of AirComp matches well with the model aggregation process in federated learning, the authors in [11]–[14] leveraged the advantages of AirComp to accelerate the convergence rate of federated learning over wireless networks. On the other hand, there were also existing studies on digital AirComp. Zhu *et al.* [15] proposed a one-bit digital AirComp scheme to facilitate communication-efficient federated learning in wideband wireless networks. Goldenbaum *et al.* [16] proposed a digital AirComp scheme to achieve the reliable computation of nomographic functions. However, the digital AirComp generally performed worse than the analog AirComp in terms of the signal distortion [17].

The efficiency of WPT can be enhanced by EB [25], which has been widely studied under the topic of wireless-powered communication networks (WPCNs) [26]–[31]. In particular, Ng *et al.* [26] formulated an energy efficiency maximization problem for orthogonal frequency division multiple access (OFDMA) systems with simultaneous wireless information and power transfer (SWIPT), and proposed an algorithm based on fractional programming and dual decomposition. Ju and Zhang [27] and Liu *et al.* [28] maximized the throughput of WPCNs by jointly optimizing the time allocated for energy harvesting and the energy beamformers. In [29], the closed-form expressions of the energy shortage probability were analyzed for SWIPT with different knowledge of CSI. In addition, Choi *et al.* [30] implemented a practical multiantenna WPCN testbed to verify the feasibility of WPT and developed a receive power-based channel estimation algorithm for WPCNs. A collaborative EB scheme was proposed in [31] to coordinate the beamforming of multiple power beacons to simultaneously power multiple sensors. We note that all the aforementioned studies on EB focused on the rate and energy efficiency maximization.

The topic of IRS has recently attracted much research interests [32]–[40]. An IRS, as a planar surface consisting of many passive and low-cost reflecting elements, can be software controlled to alter the propagation of the signals to be reflected. By adaptively controlling all reflecting elements, the IRS can introduce a desired phase shift on the incident signals. Different from the traditional full-duplex amplify-and-forward relay that relies on RF chains to amplify and regenerate the received signals, the IRS merely reflects the incident signals in a passive manner and does not consume any transmit power. In addition, the full-duplex relay suffers from severe self-interference, which needs to be mitigated by adopting advanced interference cancelation techniques and is, however, not an issue of the IRS. Obtaining accurate CSI is critical for effective beamforming optimization in IRS-aided wireless networks. By exploiting the spatial correlation property, Yang *et al.* [32] proposed a low-overhead channel estimation method for IRS-enhanced wideband communication systems, where the adjacent reflecting elements at the IRS are grouped to share the same reflection coefficient. By leveraging the sparsity of cascaded channels, Xia and Shi [33] proposed a joint activity detection and channel estimation algorithm for IRS-aided IoT networks. With perfect CSI, Jiang and Shi [34] proposed to enhance the performance of AirComp with the help of an IRS. For IRS-empowered SWIPT systems, a semidefinite relaxation (SDR)-based algorithm was proposed in [35] to maximize the weighted sum power harvested by devices. Besides, the IRS was also utilized to maximize the secrecy rate and energy efficiency in [36] and [37] by jointly designing the active and passive beamformers. The overall network power consumption of downlink nonorthogonal multiple access systems [38] and green edge inference networks [39] can be significantly reduced with the assistance of an IRS. Huang *et al.* [40] proposed a deep reinforcement learning-based method to simultaneously optimize the beamforming vector and IRS phase shifts for sum-rate maximization. However, all the aforementioned studies focused on the beamforming design for IRS-aided wireless networks either in the uplink or downlink. In addition, wireless-powered AirComp in IRS-aided IoT networks demands the joint design of downlink EB and uplink AirComp as well as the phase shifts at the IRS, which remains unexplored to the best of our knowledge.

B. Contributions

In this article, we exploit the advantages of the IRS to enhance the performance of wireless-powered data aggregation in IoT networks, where a multiantenna access point (AP) powers the IoT devices via downlink EB and the IoT devices report their data to the AP via uplink AirComp. Both the downlink EB and uplink AirComp are assisted by an IRS. With AirComp, the AP is interested in recovering a nomographic function of the aggregated data, instead of the individual data of each IoT device. The performance of uplink AirComp is characterized by the signal distortion, which is measured by the mean-squared error (MSE). It is challenging to develop an efficient algorithm to minimize the MSE in such a network setting. Specifically, the energy harvested by each IoT device in the downlink depends on both the EB vector at the AP and the downlink phase-shift matrix at the IRS. Meanwhile, the AirComp distortion in the uplink depends on both the transmit power of each IoT device and the uplink phase-shift matrix

at the IRS. The downlink and uplink transmissions are coupled as the transmit power of each IoT device is limited by the harvested energy. Moreover, the energy/aggregation beamformers and the downlink/uplink phase-shift matrices are also coupled due to the existence of the IRS. As a result, it is necessary to jointly optimize the downlink EB, uplink AirComp, and IRS phase shifts for MSE minimization in IRS-aided IoT networks with wireless-powered AirComp. The main contributions of this article are summarized as follows.

1) We formulate an MSE minimization problem to jointly optimize the energy and aggregation beamformers at the AP, the downlink/uplink phase-shift matrices at the IRS, and the transmit power at the IoT devices. However, the formulated problem is a highly intractable nonconvex quadratic programming problem, which is complicated due to the coupling between the downlink and uplink transmission as well as the coupling between the beamformers and phase-shift matrices.
2) We obtain the closed-form expressions of the energy beamformer and the device transmit power without compromising optimality, resulting in a nonconvex quadratically constrained quadratic programming (QCQP) problem. To decouple downlink EB and uplink AirComp, we propose an alternating minimization method to update the aggregation beamformer and the downlink/uplink phase-shift matrices alternately. For each update, we recast the nonconvex QCQP problem as a rank-constrained semidefinite programming (SDP) problem, which is then solved by utilizing the SDR technique. Note that the SDR method returns suboptimal solutions that fail to satisfy the rank-one constraints with a high probability, especially when the optimization variables are of high dimensions.
3) We reformulate the SDP problem with rank-one constraints as a difference-of-convex (DC) programming problem by introducing a DC representation for rank-one constraints. The DC representation is adopted to guarantee the accurate detection of the feasibility of rank-one constraints and induce the exact rank-one solutions. In addition, we develop a unified representation of the DC functions in terms of the difference of two strongly convex functions and propose an alternating DC algorithm that updates the variables via successive convex approximation to efficiently solve the original problem. Furthermore, we prove the convergence of the proposed DC algorithm.

We present the numerical results to demonstrate that deploying an IRS can substantially reduce the AirComp distortion. The proposed alternating DC algorithm achieves a better performance than the alternating SDR algorithm. Results also show the superior performance gain of the joint uplink/downlink design over the separate design in terms of minimizing the MSE.

C. Organization and Notations

The remainder of this article is organized as follows. Section II describes the system model and problem formulation. Section III presents an alternating minimization method. In Section IV, we propose an alternating DC algorithm to solve the problem. The simulation results are provided in Section V. Finally, Section VI concludes this article.

Italic, boldface lowercase, and boldface uppercase letters denote scalar, vector, and matrix, respectively. $\mathbb{C}^{m\times n}$ denotes the complex domain with the space of $m \times n$. The operators $(\cdot)^{\mathsf{T}}$, $(\cdot)^{\mathsf{H}}$, $\mathrm{Tr}(\cdot)$, and $\mathrm{diag}(\cdot)$ denote the transpose, Hermitian transpose, trace, and diagonal matrix, respectively. $\mathbb{E}[\cdot]$ denotes the statistical expectation. The operators $|\cdot|$, $\|\cdot\|$, $\|\cdot\|_2$, $\|\cdot\|_{\mathrm{F}}$, and $\|\cdot\|_*$ denote the absolute value, Euclidean norm, spectral norm, Frobenius norm, and nuclear norm, respectively. $\Re[\cdot]$ denotes the real part of a complex value.

II. System Model and Problem Formulation

In this section, we shall present the system model and formulate an MSE minimization problem for an IRS-aided IoT network supporting downlink WPT and uplink WDA.

A. System Model

Consider an IRS-aided IoT network consisting of one M-antenna AP, K single-antenna IoT devices, and one IRS, as shown in Fig. 1. The AP is multifunctional, acting as a power beacon in the downlink and a data fusion center in the uplink. We denote $\mathcal{K} = \{1, 2, \ldots, K\}$ as the index set of IoT devices that have data to be reported to the AP. Equipped with N passive reflecting elements, the IRS is deployed to assist the wireless information and power transfer between the AP and the IoT devices. By assuming that each IoT device has an RF energy harvesting module, the IoT devices operate in a harvest-then-transmit fashion. The time is slotted into a constant duration of length T. Specifically, each time slot is composed of two phases, i.e., a *downlink EB phase* of duration T_{EB} and an *uplink AirComp phase* of duration T_{AC}, where $T_{\mathrm{EB}} + T_{\mathrm{AC}} = T$.

It is worth noting that acquiring accurate CSI is critical to unleash the full potential of IRS. Although it is generally difficult to perform channel estimation for IRS-aided wireless networks, various effective channel estimation methods, taking into account the passive nature of the IRS, have recently been proposed in [32], [33], and [41]. With these effective channel estimation methods, we in this article assume that the perfect CSI is available, similar to [34]–[40], and focus on exploiting the advantages of IRS to enhance the performance of wireless-powered AirComp in IoT networks. We consider block fading for all channels, i.e., the channel coefficients remain invariant within one time slot. Although channel reciprocity is often assumed in the literature, we consider a general case that the channel responses between a pair of devices in the downlink and uplink can be different. The detailed descriptions of the downlink EB phase and the uplink AirComp phase are provided as follows.

1) Downlink EB Phase: In the downlink, the AP acts as a power beacon and delivers the power to all the IoT devices via EB with the assistance of the IRS. We denote the diagonal phase-shift matrix of the IRS during the downlink EB phase by $\boldsymbol{\Theta}_{\mathrm{D}} = \mathrm{diag}(\kappa e^{j\theta_{\mathrm{D},1}}, \kappa e^{j\theta_{\mathrm{D},2}}, \ldots, \kappa e^{j\theta_{\mathrm{D},N}}) \in \mathbb{C}^{N\times N}$, where $\kappa \in$

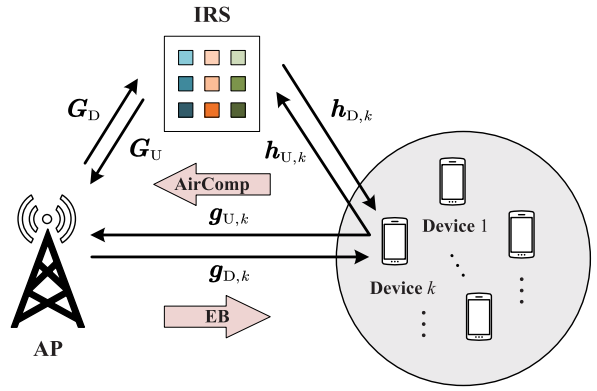

Fig. 1. Illustration of an IRS-aided IoT network with downlink EB and uplink AirComp.

$[0, 1]$ is the amplitude reflection coefficient and $\theta_{\mathrm{D},n} \in [0, 2\pi)$ denotes the phase shift of element $n \in \mathcal{N} = \{1, 2, \ldots, N\}$. As the IRS is designed to maximize the signal reflection, we assume that $\kappa = 1$ as in most of the existing works [32]–[42]. We denote $\boldsymbol{\omega}_k \in \mathbb{C}^M$ as the downlink beamforming vector at the AP for IoT device k. By assuming that the energy beams generated by the AP are typically sharp, the energy harvested from the side lobes of unintended beams is negligible and can be ignored [21]. As a result, the energy harvested by IoT device k during the downlink EB phase can be expressed as

$$E_k = \alpha_k \left| \left(\boldsymbol{h}_{\mathrm{D},k}^{\mathsf{H}} \boldsymbol{\Theta}_{\mathrm{D}} \boldsymbol{G}_{\mathrm{D}} + \boldsymbol{g}_{\mathrm{D},k}^{\mathsf{H}} \right) \boldsymbol{\omega}_k \right|^2 T_{\mathrm{EB}} \quad \forall k \in \mathcal{K} \tag{1}$$

where α_k denotes the efficiency factor of the energy conversion at IoT device k. In addition, $\boldsymbol{h}_{\mathrm{D},k} \in \mathbb{C}^N$, $\boldsymbol{G}_{\mathrm{D}} \in \mathbb{C}^{N \times M}$, and $\boldsymbol{g}_{\mathrm{D},k} \in \mathbb{C}^M$ denote the channel responses from the IRS to IoT device k, from the AP to the IRS, and from the AP to IoT device k, respectively. By denoting the maximum transmit power of the AP as $P_{\max}$, the total power constraint can be expressed as

$$\sum_{k=1}^{K} \|\boldsymbol{\omega}_k\|^2 \leq P_{\max}. \tag{2}$$

2) Uplink AirComp Phase: In the uplink, all IoT devices report their data to the AP via AirComp with the assistance of the IRS, as shown in Fig. 2. Specifically, all IoT devices simultaneously transmit their data to the AP, which aims to recover a desired function (e.g., arithmetic mean [7]) of the aggregated data, rather than the individual data of each IoT device. All IoT devices are considered to be synchronized to a common reference clock [43]. We denote $x_k \in \mathbb{C}$ as the data generated by IoT device k. The desired function at the AP can be expressed as

$$y = \phi\left(\sum_{k=1}^{K} \psi_k(x_k) \right) \tag{3}$$

where $\phi(\cdot)$ and $\psi_k(\cdot)$ denote the post-processing function at the AP and the preprocessing function at IoT device k, respectively. We denote $s_k = \psi_k(x_k)$ as the signal transmitted by IoT device k. To facilitate the computation of the desired function in (3), the AP aims to recover the function variable $s = \sum_{k=1}^{K} s_k$. Without loss of generality, we assume that $\{s_k, k \in \mathcal{K}\}$ have zero mean and unit power, i.e., $\mathbb{E}[s_k] = 0$ and $\mathbb{E}[s_k s_k^{\mathsf{H}}] = 1 \quad \forall\, k$.

We denote $\boldsymbol{\Theta}_{\mathrm{U}} = \mathrm{diag}(\kappa e^{j\theta_{\mathrm{U},1}}, \kappa e^{j\theta_{\mathrm{U},2}}, \ldots, \kappa e^{j\theta_{\mathrm{U},N}}) \in \mathbb{C}^{N \times N}$ as the diagonal phase shift matrix of the IRS during the uplink AirComp phase, where $\theta_{\mathrm{U},n} \in [0, 2\pi)$ denotes the phase shift of reflecting element $n \in \mathcal{N}$. In addition, we denote $\boldsymbol{h}_{\mathrm{U},k} \in \mathbb{C}^N$, $\boldsymbol{G}_{\mathrm{U}} \in \mathbb{C}^{M \times N}$, and $\boldsymbol{g}_{\mathrm{U},k} \in \mathbb{C}^M$ as the channel responses from IoT device k to the IRS, from the IRS to the AP, and from IoT device k to the AP, respectively. Thus, the signal received at the AP can be written as

$$\boldsymbol{y} = \sum_{k=1}^{K} \left(\boldsymbol{G}_{\mathrm{U}} \boldsymbol{\Theta}_{\mathrm{U}} \boldsymbol{h}_{\mathrm{U},k} + \boldsymbol{g}_{\mathrm{U},k} \right) \beta_k s_k + \boldsymbol{n} \tag{4}$$

where $\beta_k \in \mathbb{C}$ denotes the transmitter scalar of IoT device k and $\boldsymbol{n} \in \mathbb{C}^M$ denotes the additive white Gaussian noise (AWGN) with zero mean and variance $\sigma^2 \boldsymbol{I}$.

Each IoT device utilizes the energy harvested during the downlink EB phase to transmit data in the uplink AirComp phase. Thus, the transmit power constraint of IoT device k can be expressed as

$$|\beta_k|^2 \leq \frac{\mu_k \alpha_k T_{\mathrm{EB}}}{T_{\mathrm{AC}}} \left| \left(\boldsymbol{h}_{\mathrm{D},k}^{\mathsf{H}} \boldsymbol{\Theta}_{\mathrm{D}} \boldsymbol{G}_{\mathrm{D}} + \boldsymbol{g}_{\mathrm{D},k}^{\mathsf{H}} \right) \boldsymbol{\omega}_k \right|^2 \quad \forall k \in \mathcal{K} \tag{5}$$

where $\mu_k \in (0, 1]$ denotes the fraction of the harvested energy allocated for data transmission at device k. The distortion of the function variable (i.e., s) at the AP due to the channel noise can be mitigated by utilizing aggregation beamforming. By denoting $\boldsymbol{v} \in \mathbb{C}^M$ as the aggregation beamforming vector at the AP, the estimated function variable $\hat{s} = (1/\sqrt{\eta}) \boldsymbol{v}^{\mathsf{H}} \boldsymbol{y}$ can be written as

$$\hat{s} = \frac{1}{\sqrt{\eta}} \boldsymbol{v}^{\mathsf{H}} \sum_{k=1}^{K} \left(\boldsymbol{G}_{\mathrm{U}} \boldsymbol{\Theta}_{\mathrm{U}} \boldsymbol{h}_{\mathrm{U},k} + \boldsymbol{g}_{\mathrm{U},k} \right) \beta_k s_k + \frac{1}{\sqrt{\eta}} \boldsymbol{v}^{\mathsf{H}} \boldsymbol{n} \tag{6}$$

where η is a normalization factor.

B. Problem Formulation

We quantify the distortion of $\hat{s}$ with respect to s by MSE, which is commonly adopted to evaluate the performance of AirComp and defined as

$$\mathrm{MSE}(\hat{s}, s) = \mathbb{E}\left[|\hat{s} - s|^2 \right]. \tag{7}$$

By substituting (6) into (7), we have

$$\mathrm{MSE}(\hat{s}, s) = \sum_{k=1}^{K} \left| \frac{1}{\sqrt{\eta}} \boldsymbol{v}^{\mathsf{H}} \boldsymbol{f}_{\mathrm{U},k} \beta_k - 1 \right|^2 + \frac{\sigma^2 \|\boldsymbol{v}\|^2}{\eta} \tag{8}$$

where $\boldsymbol{f}_{\mathrm{U},k} = \boldsymbol{G}_{\mathrm{U}} \boldsymbol{\Theta}_{\mathrm{U}} \boldsymbol{h}_{\mathrm{U},k} + \boldsymbol{g}_{\mathrm{U},k}$ denotes the concatenated channel response from IoT device k to the AP.

Based on the above discussions, the MSE minimization problem can be formulated as

$$\mathscr{P}_0 : \underset{\substack{\{\boldsymbol{\omega}_k\}, \eta, \boldsymbol{\Theta}_{\mathrm{D}} \\ \boldsymbol{v}, \boldsymbol{\Theta}_{\mathrm{U}}, \{\beta_k\}}}{\text{minimize}} \sum_{k=1}^{K} \left| \frac{1}{\sqrt{\eta}} \boldsymbol{v}^{\mathsf{H}} \boldsymbol{f}_{\mathrm{U},k} \beta_k - 1 \right|^2 + \frac{\sigma^2 \|\boldsymbol{v}\|^2}{\eta} \tag{9a}$$

$$\text{subject to} \quad |\beta_k|^2 \leq \zeta_k \left| \boldsymbol{f}_{\mathrm{D},k} \boldsymbol{\omega}_k \right|^2 \quad \forall k \in \mathcal{K} \tag{9b}$$

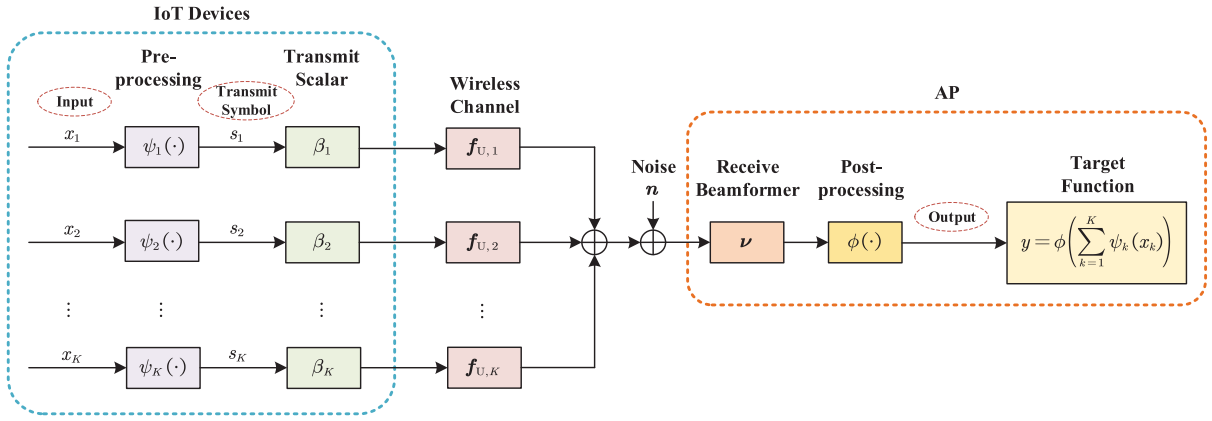

Fig. 2. Illustration of uplink AirComp in IoT networks.

$$\sum_{k=1}^{K} \|\boldsymbol{\omega}_k\|^2 \le P_{\max} \tag{9c}$$

$$\left|(\boldsymbol{\Theta}_{\mathrm{D}})_{n,n}\right| = 1 \quad \forall n \in \mathcal{N} \tag{9d}$$

$$\left|(\boldsymbol{\Theta}_{\mathrm{U}})_{n,n}\right| = 1 \quad \forall n \in \mathcal{N} \tag{9e}$$

where $\boldsymbol{f}_{\mathrm{D},k} = \boldsymbol{h}_{\mathrm{D},k}^{\mathsf{H}} \boldsymbol{\Theta}_{\mathrm{D}} \boldsymbol{G}_{\mathrm{D}} + \boldsymbol{g}_{\mathrm{D},k}^{\mathsf{H}}$ and $\zeta_k = [(\mu_k \alpha_k T_{\mathrm{EB}})/(T_{\mathrm{AC}})]$. Constraint (9b) ensures that each IoT device harvests enough energy in the downlink to support the data transmission in the uplink, indicating the coupling between the downlink and uplink transmission. Constraint (9c) represents the maximum transmit power constraint of the AP. In addition, (9d) and (9e) ensure that each reflecting element satisfies the unit modulus constraints in both the downlink and uplink.

Problem $\mathscr{P}_0$ is highly intractable due to the nonconvexity of its objective function and constraints. In particular, the optimization variables for the downlink EB phase and uplink AirComp phase are coupled in both objective function (9a) and constraint (9b). Moreover, the transmit and aggregation beamforming vectors are coupled with the downlink and uplink phase-shift matrices, respectively. To tackle these challenges and facilitate the algorithm design, we need to reformulate and simplify the optimization problem $\mathscr{P}_0$.

The following lemma presents the optimal transmit scalar of each IoT device that minimizes the MSE.

Lemma 1: Given the aggregation beamforming vector $\boldsymbol{v}$, the uplink/downlink phase-shift matrices $\boldsymbol{\Theta}_{\mathrm{U}}$ and $\boldsymbol{\Theta}_{\mathrm{D}}$, and the EB vectors $\{\boldsymbol{\omega}_k\}$, the optimal transmit scalar of IoT device k that minimizes the MSE [34] is given by

$$\beta_k^{\star} = \sqrt{\eta} \frac{1}{\boldsymbol{v}^{\mathsf{H}} \boldsymbol{f}_{\mathrm{U},k}} = \sqrt{\eta} \frac{\left(\boldsymbol{v}^{\mathsf{H}} \boldsymbol{f}_{\mathrm{U},k}\right)^{\mathsf{H}}}{\left|\boldsymbol{v}^{\mathsf{H}} \boldsymbol{f}_{\mathrm{U},k}\right|^2} \quad \forall k \in \mathcal{K} \tag{10}$$

where η can be calculated by

$$\eta = \min_k \ \zeta_k \left|\boldsymbol{f}_{\mathrm{D},k} \boldsymbol{\omega}_k\right|^2 \left|\boldsymbol{v}^{\mathsf{H}} \boldsymbol{f}_{\mathrm{U},k}\right|^2. \tag{11}$$

Proof: Refer to Appendix A. ■

By substituting (11) into (9a), we have

$$\begin{aligned} \underset{\{\boldsymbol{\omega}_k\}, \boldsymbol{\Theta}_{\mathrm{D}}, \boldsymbol{v}, \boldsymbol{\Theta}_{\mathrm{U}}}{\text{minimize}} \quad & \max_k \frac{\|\boldsymbol{v}\|^2}{\zeta_k \left|\boldsymbol{f}_{\mathrm{D},k} \boldsymbol{\omega}_k\right|^2 \left|\boldsymbol{v}^{\mathsf{H}} \boldsymbol{f}_{\mathrm{U},k}\right|^2} \\ \text{subject to} \quad & \text{constraints (9c)–(9e).} \end{aligned} \tag{12}$$

The following lemma presents the optimal transmit beamforming vector at the AP in the downlink.

Lemma 2: The optimal EB vector at the AP should be aligned with the direction of the downlink composite channel, i.e.,

$$\boldsymbol{\omega}_k^{\star} = \frac{\boldsymbol{f}_{\mathrm{D},k}^{\mathsf{H}}}{\left\|\boldsymbol{f}_{\mathrm{D},k}\right\|} \sqrt{P_k} \tag{13}$$

where P_k denotes transmit power allocated to IoT device k at the AP.

Proof: In order to minimize the objective function in (12), $\boldsymbol{\omega}_k$ should be selected to maximize the denominator. As $|\boldsymbol{f}_{\mathrm{D},k} \boldsymbol{\omega}_k|^2 \le \|\boldsymbol{f}_{\mathrm{D},k}\|^2 \|\boldsymbol{\omega}_k\|^2$ with the equality holds if and only if the EB has the same direction as $\boldsymbol{f}_{\mathrm{D},k}$, the optimal EB vector can be directly obtained as in (13). ■

By substituting (13) into (12), we have

$$\underset{\boldsymbol{\Theta}_{\mathrm{D}}, \boldsymbol{v}, \boldsymbol{\Theta}_{\mathrm{U}}, \{P_k\}}{\text{minimize}} \quad \max_k \frac{\|\boldsymbol{v}\|^2}{\zeta_k P_k \left\|\boldsymbol{f}_{\mathrm{D},k}\right\|^2 \left|\boldsymbol{v}^{\mathsf{H}} \boldsymbol{f}_{\mathrm{U},k}\right|^2} \tag{14a}$$

$$\text{subject to} \quad \sum_{k=1}^{K} P_k \le P_{\max} \tag{14b}$$

$$\text{constraints (9d) and (9e).} \tag{14c}$$

To facilitate the algorithm design, we further rewrite problem (14) in the following proposition.

Proposition 1: Problem (14) can be equivalently reformulated as the following optimization problem:

$$\underset{\boldsymbol{\Theta}_{\mathrm{D}}, \boldsymbol{v}, \boldsymbol{\Theta}_{\mathrm{U}}, \{P_k\}}{\text{minimize}} \quad \|\boldsymbol{v}\|^2 \tag{15a}$$

$$\text{subject to} \quad \zeta_k P_k \|\boldsymbol{f}_{\mathrm{D},k}\|^2 |\boldsymbol{v}^{\mathsf{H}} \boldsymbol{f}_{\mathrm{U},k}|^2 \ge 1 \quad \forall k \in \mathcal{K} \tag{15b}$$

$$\text{constraints (9d), (9e), (14b).} \tag{15c}$$

Proof: Refer to Appendix B. ■

After combining constraints (14b) and (15b), problem (14) can be further written as

$$\begin{aligned} \mathscr{P}: \ \underset{\boldsymbol{\Theta}_{\mathrm{D}}, \boldsymbol{v}, \boldsymbol{\Theta}_{\mathrm{U}}}{\text{minimize}} \quad & \|\boldsymbol{v}\|^2 \\ \text{subject to} \quad & \sum_{k=1}^{K} \frac{1}{\zeta_k P_{\max} \left\|\boldsymbol{f}_{\mathrm{D},k}\right\|^2 \left|\boldsymbol{v}^{\mathsf{H}} \boldsymbol{f}_{\mathrm{U},k}\right|^2} \le 1 \\ & \text{constraints (9d) and (9e).} \end{aligned} \tag{16}$$

Problem $\mathscr{P}$ is still highly intractable due to the nonconvex quadratic constraints with respect to $\boldsymbol{v}$, $\boldsymbol{\Theta}_{\mathrm{D}}$, and $\boldsymbol{\Theta}_{\mathrm{U}}$. In the following section, we shall propose an alternating minimization approach to solve problem $\mathscr{P}$.

III. Alternating Minimization Method

In this section, we alternately optimize aggregation beamforming vector $\boldsymbol{v}$, uplink phase-shift matrix $\boldsymbol{\Theta}_{\mathrm{U}}$, and downlink phase-shift matrix $\boldsymbol{\Theta}_{\mathrm{D}}$ to solve problem $\mathscr{P}$.

A. Alternating Optimization

Given the downlink and uplink phase-shift matrices $\boldsymbol{\Theta}_{\mathrm{D}}$ and $\boldsymbol{\Theta}_{\mathrm{U}}$, problem $\mathscr{P}$ can be simplified as

$$\begin{aligned} \underset{\boldsymbol{v}}{\text{minimize}} \quad & \|\boldsymbol{v}\|^2 \\ \text{subject to} \quad & \sum_{k=1}^{K} \frac{1}{C_{1,k}\left|\boldsymbol{v}^{\mathsf{H}}\boldsymbol{f}_{\mathrm{U},k}\right|^2} \leq 1 \end{aligned} \tag{17}$$

where $C_{1,k} = \zeta_k P_{\max}\|\boldsymbol{f}_{\mathrm{D},k}\|^2$.

Given the aggregation beamforming vector $\boldsymbol{v}$ and the downlink phase-shift matrix $\boldsymbol{\Theta}_{\mathrm{D}}$, problem $\mathscr{P}$ reduces to a feasibility detection problem. Specifically, by denoting $\boldsymbol{z} = [e^{j\theta_{\mathrm{U},1}}, \ldots, e^{j\theta_{\mathrm{U},N}}]^{\mathsf{T}}$, $\boldsymbol{a}_{1,k}^{\mathsf{H}} = \boldsymbol{v}^{\mathsf{H}}\boldsymbol{G}_{\mathrm{U}}\mathrm{diag}(\boldsymbol{h}_{\mathrm{U},k})$, and $c_k = \boldsymbol{v}^{\mathsf{H}}\boldsymbol{g}_{\mathrm{U},k}$, problem $\mathscr{P}$ can be written as

$$\begin{aligned} \text{find} \quad & \boldsymbol{z} \\ \text{subject to} \quad & \sum_{k=1}^{K} \frac{1}{C_{1,k}\left|\boldsymbol{a}_{1,k}^{\mathsf{H}}\boldsymbol{z} + c_k\right|^2} \leq 1 \\ & |z_n|^2 = 1 \quad \forall n \in \mathcal{N}. \end{aligned} \tag{18}$$

Problem (18) can be further transformed to the following nonconvex homogeneous QCQP problem:

$$\begin{aligned} \text{find} \quad & \tilde{\boldsymbol{z}} \\ \text{subject to} \quad & \sum_{k=1}^{K} \frac{1}{C_{1,k}\left(\tilde{\boldsymbol{z}}^{\mathsf{H}}\boldsymbol{R}_k\tilde{\boldsymbol{z}} + |c_k|^2\right)} \leq 1 \\ & |\tilde{z}_n|^2 = 1 \quad \forall n \in \{1, \ldots, N+1\} \end{aligned} \tag{19}$$

where

$$\boldsymbol{R}_k = \begin{bmatrix} \boldsymbol{a}_{1,k}\boldsymbol{a}_{1,k}^{\mathsf{H}}, & \boldsymbol{a}_{1,k}c_k \\ c_k^{\mathsf{H}}\boldsymbol{a}_{1,k}^{\mathsf{H}}, & 0 \end{bmatrix}, \ \tilde{\boldsymbol{z}} = \begin{bmatrix} \boldsymbol{z} \\ t_1 \end{bmatrix} \tag{20}$$

and t_1 is an auxiliary variable. If a feasible solution $\tilde{\boldsymbol{z}}^{\star} = [\hat{\boldsymbol{z}}, \hat{t}_1]^{\mathsf{T}}$ to problem (19) is obtained, then we can get a feasible solution to problem (18) as $\boldsymbol{z}^{\star} = \hat{\boldsymbol{z}}/\hat{t}_1$, which can be used to recover the uplink phase-shift matrix by setting $\boldsymbol{\Theta}_{\mathrm{U}} = \mathrm{diag}(\boldsymbol{z}^{\star})$.

Given the aggregation beamforming vector $\boldsymbol{v}$ and the uplink phase-shift matrix $\boldsymbol{\Theta}_{\mathrm{U}}$, problem $\mathscr{P}$ is also a feasibility detection problem. Similarly, by denoting $\boldsymbol{q} = [e^{-j\theta_{\mathrm{D},1}}, \ldots, e^{-j\theta_{\mathrm{D},N}}]^{\mathsf{T}}$ and $\boldsymbol{a}_{2,k} = \mathrm{diag}(\boldsymbol{h}_{\mathrm{D},k}^{\mathsf{H}})\boldsymbol{G}_{\mathrm{D}}$, problem $\mathscr{P}$ can be simplified as

$$\begin{aligned} \text{find} \quad & \boldsymbol{q} \\ \text{subject to} \quad & \sum_{k=1}^{K} \frac{1}{C_{2,k}\|\boldsymbol{q}^{\mathsf{H}}\boldsymbol{a}_{2,k} + \boldsymbol{g}_{\mathrm{D},k}^{\mathsf{H}}\|^2} \leq 1 \\ & |q_n|^2 = 1 \quad \forall n \in \mathcal{N} \end{aligned} \tag{21}$$

where $C_{2,k} = \zeta_k P_{\max}|\boldsymbol{v}^{\mathsf{H}}\boldsymbol{f}_{\mathrm{U},k}|^2$. Problem (21) can be further transformed to the following nonconvex homogeneous QCQP problem:

$$\begin{aligned} \text{find} \quad & \tilde{\boldsymbol{q}} \\ \text{subject to} \quad & \sum_{k=1}^{K} \frac{1}{C_{2,k}\|\tilde{\boldsymbol{q}}^{\mathsf{H}}\boldsymbol{b}_k\|^2} \leq 1 \\ & |\tilde{q}_n|^2 = 1 \quad \forall n \in \{1, \ldots, N+1\} \end{aligned} \tag{22}$$

where $\tilde{\boldsymbol{q}} = [\boldsymbol{q}, t_2]^{\mathsf{T}}$, $\boldsymbol{b}_k = [\boldsymbol{a}_{2,k}, \boldsymbol{g}_{\mathrm{D},k}^{\mathsf{H}}]^{\mathsf{T}}$, and t_2 is an auxiliary variable. We obtain a feasible solution $\boldsymbol{q}^{\star} = \hat{\boldsymbol{q}}/\hat{t}_2$ to problem (21) after getting a feasible solution, denoted as $\tilde{\boldsymbol{q}}^{\star} = [\hat{\boldsymbol{q}}, \hat{t}_2]^{\mathsf{T}}$, to problem (22). The downlink phase-shift matrix can be recovered as $\boldsymbol{\Theta}_{\mathrm{D}} = \mathrm{diag}((\boldsymbol{q}^{\star})^{\mathsf{H}})$, where the diagonal entries of matrix $\boldsymbol{\Theta}_{\mathrm{D}}$ are the conjugate of vector $\boldsymbol{q}^{\star}$.

In summary, we solve problem $\mathscr{P}$ by alternately solving problems (17), (19), and (22), which are all nonconvex QCQP problems and can be further transformed to SDP problems via matrix lifting in the following section.

B. Matrix Lifting

To tackle the nonconvexity of problems (17), (19), and (22), we reformulate them as SDP problems via matrix lifting [44]. We denote $\boldsymbol{V} = \boldsymbol{v}\boldsymbol{v}^{\mathsf{H}}$, which is a symmetric positive semidefinite (PSD) matrix with rank one. As a result, problem (17) can be rewritten as

$$\begin{aligned} \mathscr{P}_1: \ \underset{\boldsymbol{V}}{\text{minimize}} \quad & \mathrm{Tr}(\boldsymbol{V}) \\ \text{subject to} \quad & \sum_{k=1}^{K} \frac{1}{C_{1,k}\mathrm{Tr}(\boldsymbol{V}\boldsymbol{F}_k)} \leq 1 \\ & \boldsymbol{V} \succeq 0, \ \mathrm{rank}(\boldsymbol{V}) = 1 \end{aligned} \tag{23}$$

where $\boldsymbol{F}_k = \boldsymbol{f}_{\mathrm{U},k}\boldsymbol{f}_{\mathrm{U},k}^{\mathsf{H}}$.

Similarly, problems (19) and (22) can also be equivalently reformulated as rank-one matrix optimization problem. Specifically, by denoting $\boldsymbol{Z} = \tilde{\boldsymbol{z}}\tilde{\boldsymbol{z}}^{\mathsf{H}}$, $\boldsymbol{Q} = \tilde{\boldsymbol{q}}\tilde{\boldsymbol{q}}^{\mathsf{H}}$, and $\boldsymbol{B}_k = \boldsymbol{b}_k\boldsymbol{b}_k^{\mathsf{H}}$, problems (19) and (22) can, respectively, be reformulated as

$$\begin{aligned} \mathscr{P}_2: \ \text{find} \quad & \boldsymbol{Z} \\ \text{subject to} \quad & \sum_{k=1}^{K} \frac{1}{C_{1,k}\left(\mathrm{Tr}(\boldsymbol{R}_k\boldsymbol{Z}) + |c_k|^2\right)} \leq 1 \\ & \boldsymbol{Z}_{n,n} = 1 \quad \forall n \in \{1, \ldots, N+1\} \\ & \boldsymbol{Z} \succeq 0, \ \mathrm{rank}(\boldsymbol{Z}) = 1 \end{aligned} \tag{24}$$

and

$$\begin{aligned} \mathscr{P}_3: \ \text{find} \quad & \boldsymbol{Q} \\ \text{subject to} \quad & \sum_{k=1}^{K} \frac{1}{C_{2,k}\mathrm{Tr}(\boldsymbol{Q}\boldsymbol{B}_k)} \leq 1 \\ & \boldsymbol{Q}_{n,n} = 1 \quad \forall n \in \{1, \ldots, N+1\} \\ & \boldsymbol{Q} \succeq 0, \ \mathrm{rank}(\boldsymbol{Q}) = 1. \end{aligned} \tag{25}$$

After reformulating problems (17), (19), and (22) as problems $\mathscr{P}_1$, $\mathscr{P}_2$, and $\mathscr{P}_3$, respectively, the lack of convexity arises only from the rank-one constraints. To this end, the

Algorithm 1: Alternating SDR Algorithm for Problem $\mathscr{P}$

Input: $\boldsymbol{\Theta}_{\mathrm{U}}^0$, $\boldsymbol{\Theta}_{\mathrm{D}}^0$, and predefined threshold $\epsilon > 0$.
Output: $\mathrm{MSE}^\star$.

```
for t ← 1, 2, ... do
    Given Θ_U^{t-1} and Θ_D^{t-1}, solve problem P_1 to get v^t.
    Given Θ_D^{t-1} and v^t, solve problem P_2 to get Θ_U^t.
    Given v^t and Θ_U^t, solve problem P_3 to get Θ_D^t.
    if |MSE^t − MSE^{t-1}| < ε or problem P_2 or P_3 becomes infeasible then
        MSE* = MSE^t.
        break.
    end
end
```

SDR technique can be applied to tackle this challenge by simply dropping the rank-one constraints [45]. The resulting SDP problems can be efficiently solved by using CVX [46]. It is worth noting that the optimal solution to the original problem can be obtained via Cholesky decomposition if the obtained matrix solution to the SDP problem meets the rank-one constraints. However, if the returned matrix solution of the SDP problem fails to be rank-one, then Gaussian randomization can be utilized to obtain a suboptimal solution to the original problem [44]. The proposed alternating SDR algorithm for solving problem $\mathscr{P}$ is summarized in Algorithm 1. As problems $\mathscr{P}_2$ and $\mathscr{P}_3$ are not guaranteed to be feasible, Algorithm 1 terminates when either problem $\mathscr{P}_2$ or $\mathscr{P}_3$ becomes infeasible, or the difference of MSE in consecutive iterations is smaller than a predefined threshold ϵ.

IV. Alternating Difference of Convex Algorithm

Although the alternating SDR algorithm is able to efficiently solve problem $\mathscr{P}$, the obtained solutions usually do not meet the rank-one constraints and are suboptimal, especially when the dimension of the optimization variables becomes large. To overcome the drawback of the SDR method, we, in this section propose to solve the aforementioned rank-one constrained matrix optimization problems by proposing an alternating DC algorithm. This is achieved by representing the rank-one constraints as DC functions and developing an effective alternating DC algorithm to obtain the optimal rank-one solutions via successively solving the primal and dual problems of DC functions. Moreover, we rigorously prove the convergence of the proposed DC algorithm.

A. Transformation of Rank-One Constraints

The general rank-one constrained matrix optimization problem of minimizing the trace of a matrix has the form of [44]

$$\begin{aligned} \underset{\boldsymbol{X}\in\mathcal{H}}{\text{minimize}} \quad & \mathrm{Tr}(\boldsymbol{C}\boldsymbol{X}) \\ \text{subject to} \quad & \mathrm{Tr}(\boldsymbol{A}_i\boldsymbol{X}) \succeq_i b_i \quad \forall\, i \\ & \boldsymbol{X} \succeq 0,\ \mathrm{rank}(\boldsymbol{X}) = 1 \end{aligned} \tag{26}$$

where $\boldsymbol{X} \in \mathcal{H}$ means that matrix $\boldsymbol{X}$ is Hermitian, and "$\succeq_i$" can be either "$\geq$," "$=$," or "$\leq$" for each i.

As rank-one matrix $\boldsymbol{X} \in \mathbb{C}^{N\times N}$ has only one nonzero singular value, we have

$$\left\|\{\sigma_i(\boldsymbol{X})\}_{i=1}^N\right\|_0 = 1 \Leftrightarrow \|\boldsymbol{X}\|_* = \sum_{i=1}^N \sigma_i(\boldsymbol{X}) = \sigma_1(\boldsymbol{X}) \tag{27}$$

where $\sigma_i(\boldsymbol{X})$ denotes the ith largest singular value of matrix $\boldsymbol{X}$. For a general square matrix $\boldsymbol{X}$, its spectral norm is given by

$$\|\boldsymbol{X}\|_2 = \max\{\sigma_i(\boldsymbol{X})\}_{i=1}^N = \sigma_1(\boldsymbol{X}). \tag{28}$$

With (27) and (28), an exact representation for the rank-one constraint is presented in the following proposition.

Proposition 2: For a PSD matrix $\boldsymbol{X} \in \mathbb{C}^{N\times N}$ with $\mathrm{Tr}(\boldsymbol{X}) > 0$, we have

$$\mathrm{rank}(\boldsymbol{X}) = 1 \Leftrightarrow \mathrm{Tr}(\boldsymbol{X}) - \|\boldsymbol{X}\|_2 = 0. \tag{29}$$

Proof: If a PSD matrix $\boldsymbol{X} \in \mathbb{C}^{N\times N}$ is rank-one, then we have $\mathrm{Tr}(\boldsymbol{X}) = \|\boldsymbol{X}\|_* = \sigma_1(\boldsymbol{X}) = \|\boldsymbol{X}\|_2$ as $\sigma_i(\boldsymbol{X}) = 0 \ \ \forall\, i \geq 2$. On the one hand, equation $\mathrm{Tr}(\boldsymbol{X}) - \|\boldsymbol{X}\|_2 = 0$ implies that $\mathrm{rank}(\boldsymbol{X}) = \|\{\sigma_i(\boldsymbol{X})\}_{i=1}^N\|_0 \leq 1$. On the other hand, we have $\mathrm{rank}(\boldsymbol{X}) \geq 1$ as $\mathrm{Tr}(\boldsymbol{X}) > 0$. Consequently, $\mathrm{rank}(\boldsymbol{X}) = 1$ is equivalently to $\mathrm{Tr}(\boldsymbol{X}) - \|\boldsymbol{X}\|_2 = 0$. ■

Based on Proposition 2, we can add DC function $\mathrm{Tr}(\boldsymbol{X}) - \|\boldsymbol{X}\|_2$ to the objective function of problem (26) as a penalty component as follows:

$$\begin{aligned} \underset{\boldsymbol{X}\in\mathcal{H}}{\text{minimize}} \quad & \mathrm{Tr}(\boldsymbol{C}\boldsymbol{X}) + \rho(\mathrm{Tr}(\boldsymbol{X}) - \|\boldsymbol{X}\|_2) \\ \text{subject to} \quad & \mathrm{Tr}(\boldsymbol{A}_i\boldsymbol{X}) \succeq_i b_i \quad \forall\, i \\ & \boldsymbol{X} \succeq 0 \end{aligned} \tag{30}$$

where $\rho > 0$ is the penalty parameter. We are able to obtain an exact rank-one solution when $\mathrm{Tr}(\boldsymbol{X}) - \|\boldsymbol{X}\|_2$ is enforced to be zero. Note that $\mathrm{Tr}(\boldsymbol{X}) - \|\boldsymbol{X}\|_2$ is still nonconvex as function $\mathrm{Tr}(\boldsymbol{X})$ is convex and function $-\|\boldsymbol{X}\|_2$ is concave [47].

B. Reformulation With DC Functions

With Proposition 2, we apply the DC method to reformulate problems $\mathscr{P}_1$, $\mathscr{P}_2$, and $\mathscr{P}_3$. In particular, given the downlink and uplink phase-shift matrices $\boldsymbol{\Theta}_{\mathrm{D}}$ and $\boldsymbol{\Theta}_{\mathrm{U}}$, we obtain the optimal rank-one solution of problem $\mathscr{P}_1$ by solving the following DC programming problem:

$$\begin{aligned} \underset{\boldsymbol{V}}{\text{minimize}} \quad & \mathrm{Tr}(\boldsymbol{V}) + \rho(\mathrm{Tr}(\boldsymbol{V}) - \|\boldsymbol{V}\|_2) \\ \text{subject to} \quad & \sum_{k=1}^K \frac{1}{C_{1,k}\mathrm{Tr}(\boldsymbol{V}\boldsymbol{F}_k)} \leq 1 \\ & \boldsymbol{V} \succeq 0. \end{aligned} \tag{31}$$

By minimizing the objective value of problem (31), the penalty component is enforced to be zero, which induces the optimal rank-one solution of problem $\mathscr{P}_1$. After that, we obtain the aggregation beamforming vector $\boldsymbol{v}$ via Cholesky decomposition for $\boldsymbol{V}^\star = \boldsymbol{v}\boldsymbol{v}^{\mathsf{H}}$.

Given the aggregation beamforming vector $\boldsymbol{v}$ and downlink phase-shift matrix $\boldsymbol{\Theta}_{\mathrm{D}}$, we convert the feasibility detection problem $\mathscr{P}_2$ into an optimization problem of minimizing the

difference between the trace norm and the spectral norm, given by

$$\begin{aligned} \underset{\boldsymbol{Z}}{\text{minimize}} \quad & \text{Tr}(\boldsymbol{Z}) - \|\boldsymbol{Z}\|_2 \\ \text{subject to} \quad & \sum_{k=1}^{K} \frac{1}{C_{1,k}\left(\text{Tr}(\boldsymbol{R}_k\boldsymbol{Z}) + |c_k|^2\right)} \leq 1 \\ & \boldsymbol{Z}_{n,n} = 1 \quad \forall n \in \{1, \ldots, N+1\} \\ & \boldsymbol{Z} \succeq 0. \end{aligned} \tag{32}$$

An exact rank-one feasible solution $\boldsymbol{Z}^\star$ of problem $\mathscr{P}_2$ can be found when the objective value of problem (32) becomes zero. Subsequently, a feasible solution of problem (19), denoted as $\tilde{\boldsymbol{z}}$, can be recovered according to the Cheloesky decomposition, i.e., $\boldsymbol{Z}^\star = \tilde{\boldsymbol{z}}\tilde{\boldsymbol{z}}^{\mathsf{H}}$, which in turn yields a feasible solution of problem (18), i.e., $\boldsymbol{z} = [\tilde{\boldsymbol{z}}/\tilde{z}_{N+1}]_{(1:N)}$.

Similarly, given aggregation beamforming vector $\boldsymbol{v}$ and uplink phase-shift matrix $\boldsymbol{\Theta}_{\text{U}}$, the feasibility detection problem $\mathscr{P}_3$ can be transformed into the following DC function minimization problem:

$$\begin{aligned} \underset{\boldsymbol{Q}}{\text{minimize}} \quad & \text{Tr}(\boldsymbol{Q}) - \|\boldsymbol{Q}\|_2 \\ \text{subject to} \quad & \sum_{k=1}^{K} \frac{1}{C_{2,k}\text{Tr}(\boldsymbol{Q}\boldsymbol{B}_k)} \leq 1 \\ & \boldsymbol{Q}_{n,n} = 1 \quad \forall n \in \{1, \ldots, N+1\} \\ & \boldsymbol{Q} \succeq 0. \end{aligned} \tag{33}$$

If the objective value of problem (33) becomes zero, then an exact rank-one solution $\boldsymbol{Q}^\star$ of problem (22) can be obtained. By utilizing Cholesky decomposition for $\boldsymbol{Q}^\star = \tilde{\boldsymbol{q}}\tilde{\boldsymbol{q}}^{\mathsf{H}}$, we obtain a feasible solution of problem (21), denoted as $\boldsymbol{q} = [\tilde{\boldsymbol{q}}/\tilde{\boldsymbol{q}}_{N+1}]_{(1:N)}$.

As the aforementioned DC programming problems [i.e., (31)–(33)] are still nonconvex, a unified DC representation [48] shall be developed in the following section.

C. Unified Representation of DC Functions

In this section, we represent the objective functions of problems (31)–(33) as the difference of two strongly convex functions, so as to exploit the important properties of the DC algorithm. In particular, problems (31)–(33) can be rewritten as

$$\underset{\boldsymbol{V}}{\text{minimize}} \quad f_1 = \text{Tr}(\boldsymbol{V}) + \rho(\text{Tr}(\boldsymbol{V}) - \|\boldsymbol{V}\|_2) + \mathbb{I}_{\mathcal{C}_1}(\boldsymbol{V}) \tag{34}$$

$$\underset{\boldsymbol{Z}}{\text{minimize}} \quad f_2 = \text{Tr}(\boldsymbol{Z}) - \|\boldsymbol{Z}\|_2 + \mathbb{I}_{\mathcal{C}_2}(\boldsymbol{Z}) \tag{35}$$

$$\underset{\boldsymbol{Q}}{\text{minimize}} \quad f_3 = \text{Tr}(\boldsymbol{Q}) - \|\boldsymbol{Q}\|_2 + \mathbb{I}_{\mathcal{C}_3}(\boldsymbol{Q}) \tag{36}$$

where $\mathcal{C}_1$, $\mathcal{C}_2$, and $\mathcal{C}_3$ denote the PSD cones that satisfy the constraints of problems (31), (32), and (33), and the indicator function is defined as

$$\mathbb{I}_{\mathcal{C}}(\boldsymbol{X}) = \begin{cases} 0, & \text{if } \boldsymbol{X} \in \mathcal{C} \\ +\infty, & \text{otherwise.} \end{cases} \tag{37}$$

As a result, we rewrite the DC functions in (34)–(36) as the difference of two strongly convex functions, i.e., $f_i = g_i - h_i$, $i \in \{1, 2, 3\}$, where

$$g_1 = \text{Tr}(\boldsymbol{V}) + \rho\text{Tr}(\boldsymbol{V}) + \mathbb{I}_{\mathcal{C}_1}(\boldsymbol{V}) + \frac{\gamma}{2}\|\boldsymbol{V}\|_{\text{F}}^2 \tag{38}$$

$$h_1 = \rho\|\boldsymbol{V}\|_2 + \frac{\gamma}{2}\|\boldsymbol{V}\|_{\text{F}}^2 \tag{39}$$

$$g_2 = \text{Tr}(\boldsymbol{Z}) + \mathbb{I}_{\mathcal{C}_2} + \frac{\gamma}{2}\|\boldsymbol{Z}\|_{\text{F}}^2 \tag{40}$$

$$h_2 = \|\boldsymbol{Z}\|_2 + \frac{\gamma}{2}\|\boldsymbol{Z}\|_{\text{F}}^2 \tag{41}$$

$$g_3 = \text{Tr}(\boldsymbol{Q}) + \mathbb{I}_{\mathcal{C}_3} + \frac{\gamma}{2}\|\boldsymbol{Q}\|_{\text{F}}^2 \tag{42}$$

$$h_3 = \|\boldsymbol{Q}\|_2 + \frac{\gamma}{2}\|\boldsymbol{Q}\|_{\text{F}}^2. \tag{43}$$

It is worth noting that g_i and h_i are γ-strongly convex functions with an additional quadratic term $(\gamma/2)\|\boldsymbol{X}\|_{\text{F}}^2$. With the above definitions, problems (31)–(33) can be rewritten as

$$\underset{\boldsymbol{X} \in \mathcal{C}_i}{\text{minimize}} \quad f_i = g_i(\boldsymbol{X}) - h_i(\boldsymbol{X}), \quad i \in \{1, 2, 3\}. \tag{44}$$

D. Proposed Alternating DC Algorithm

In order to solve the nonconvex problem (44), we first obtain its dual problem based on Fenchel's duality [49], given by

$$\underset{\boldsymbol{Y} \in \mathcal{Y}}{\text{minimize}} \quad f_i^* = h_i^*(\boldsymbol{Y}) - g_i^*(\boldsymbol{Y}), \quad i \in \{1, 2, 3\} \tag{45}$$

where g_i^* and h_i^* are the conjugate functions of g_i and h_i, respectively, and $\boldsymbol{Y}$ denotes the dual variable of $\boldsymbol{X}$. The conjugate function of $F(\boldsymbol{Y})$ is defined as

$$F^*(\boldsymbol{Y}) = \sup_{\boldsymbol{X} \in \mathcal{X}} \quad \langle \boldsymbol{X}, \boldsymbol{Y} \rangle - F(\boldsymbol{X}) \tag{46}$$

where the inner product is defined as $< \boldsymbol{X}, \boldsymbol{Y} >= \Re[\text{Tr}(\boldsymbol{X}^{\mathsf{H}}\boldsymbol{Y})]$ in the complex domain [50]. Subsequently, we iteratively update the primal and dual variables via SCA. At iteration t, we have

$$\boldsymbol{Y}^t = \arg\inf_{\boldsymbol{Y} \in \mathcal{Y}} h_i^*(\boldsymbol{Y}) - \left[g_i^*\left(\boldsymbol{Y}^{t-1}\right) + \left\langle \boldsymbol{Y} - \boldsymbol{Y}^{t-1}, \boldsymbol{X}^t \right\rangle\right] \tag{47}$$

$$\boldsymbol{X}^{t+1} = \arg\inf_{\boldsymbol{X} \in \mathcal{X}} g_i(\boldsymbol{X}) - \left[h_i\left(\boldsymbol{X}^t\right) + \left\langle \boldsymbol{X} - \boldsymbol{X}^t, \boldsymbol{Y}^t \right\rangle\right]. \tag{48}$$

Moreover, based on the Fenchel biconjugation theorem [49], (47) is given by $\boldsymbol{Y}^t \in \partial_{\boldsymbol{X}^t} h_i$, which is the subgradient of h_i with respect to $\boldsymbol{X}$ at iteration t. Hence, the optimal solution $\boldsymbol{X}^t$ at iteration t can be obtained by solving the following convex subproblem:

$$\underset{\boldsymbol{X}}{\text{minimize}} \quad g_i - \left\langle \boldsymbol{X}, \partial_{\boldsymbol{X}^{t-1}} h_i \right\rangle, \quad i \in \{1, 2, 3\} \tag{49}$$

where $\boldsymbol{X}^{t-1}$ is the optimal solution of problem (49) at iteration $t-1$. To be specific, we obtain the optimal solution $\boldsymbol{V}^t$ of problem (31) by solving the following convex subproblem at iteration t:

$$\underset{\boldsymbol{V}}{\text{minimize}} \quad g_1 - \left\langle \boldsymbol{V}, \partial_{\boldsymbol{V}^{t-1}} h_1 \right\rangle \tag{50}$$

where $\boldsymbol{V}^{t-1}$ is the optimal solution of the subproblem at iteration $t-1$ and $\partial_{\boldsymbol{V}^{t-1}} h_1 = \rho\partial_{\boldsymbol{V}^{t-1}}\|\boldsymbol{V}\|_2 + \gamma\boldsymbol{V}^{t-1}$. Similarly, the optimal solution $\boldsymbol{Z}^t$ of problem (32) at iteration t can be obtained by solving the following convex optimization problem:

$$\underset{\boldsymbol{Z}}{\text{minimize}} \quad g_2 - \left\langle \boldsymbol{Z}, \partial_{\boldsymbol{Z}^{t-1}} h_2 \right\rangle \tag{51}$$

Algorithm 2: DC Algorithm for Problem (30)

Input: $\boldsymbol{X}^0$, and predefined threshold $\epsilon_{\mathrm{DC}} > 0$.
Output: $\boldsymbol{X}^\star$.
for $t \leftarrow 1, 2, \ldots$ **do**
  Compute the subgradient $\partial \|\boldsymbol{X}^{t-1}\|_2$.
  Solve convex subproblem (49) to get $\boldsymbol{X}^t$.
  if *The decrease of objective value* (49) *is below* ϵ_{DC} **then**
    $\boldsymbol{X}^\star = \boldsymbol{X}^t$.
    break.
  end
end

where $\boldsymbol{Z}^{t-1}$ is the optimal solution of the subproblem at iteration $t-1$ and $\partial_{\boldsymbol{Z}^{t-1}} h_2 = \partial_{\boldsymbol{Z}^{t-1}} \|\boldsymbol{Z}\|_2 + \gamma \boldsymbol{Z}^{t-1}$. Moreover, the optimal solution $\boldsymbol{Q}^t$ of problem (33) at iteration t is given by

$$\underset{\boldsymbol{Q}}{\text{minimize}} \quad g_3 - \left\langle \boldsymbol{Q}, \partial_{\boldsymbol{Q}^{t-1}} h_3 \right\rangle \tag{52}$$

where $\boldsymbol{Q}^{t-1}$ is the optimal solution of the subproblem at iteration $t-1$ and $\partial_{\boldsymbol{Q}^{t-1}} h_3 = \partial_{\boldsymbol{Q}^{t-1}} \|\boldsymbol{Q}\|_2 + \gamma \boldsymbol{Q}^{t-1}$. It is clear that the above subproblems are all convex and can be efficiently solved by using CVX [46]. Furthermore, the following proposition provides an efficient way to compute the subgradient of the spectral norm.

Proposition 3: For a PSD matrix $\boldsymbol{X} \in \mathbb{C}^{m \times m}$, we have

$$\boldsymbol{u}_1 \boldsymbol{u}_1^{\mathsf{H}} \in \partial \|\boldsymbol{X}\|_2 \tag{53}$$

where $\boldsymbol{u}_1$ is the eigenvector corresponding to the largest eigenvalue of matrix $\boldsymbol{X}$.

Proof: Refer to Appendix C. ∎

The optimal solutions of problem (30) as well as problems (31)–(33) can be obtained by using Algorithm 2 with an arbitrary initial point $\boldsymbol{X}^0$ [48]. The proposed alternating DC algorithm for solving problem $\mathscr{P}$ is summarized in Algorithm 3. The convergence property of the DC algorithm is provided in the following proposition.

Proposition 4: The sequence $\{\boldsymbol{X}^t\}$ constructed by iteratively solving the convex subproblems (49) has following properties.

1) The sequence $\{\boldsymbol{X}^t\}$ converges to a critical point of f_i, $i \in \{1, 2, 3\}$, in (44) from an arbitrary initial point, and the sequence $\{f_i(\boldsymbol{X}^t)\}$ is strictly decreasing and convergent.
2) For any iteration $t = 1, 2, \ldots$, we have

$$\mathbb{A}\left[\left\{\left\|\boldsymbol{X}^r - \boldsymbol{X}^{r+1}\right\|_{\mathrm{F}}^2\right\}_{r=0}^{t}\right] \leq \frac{f_i(\boldsymbol{X}^0) - f_i(\boldsymbol{X}^\star)}{\gamma(t+1)} \tag{54}$$

where $\mathbb{A}[\,\cdot\,]$ computes the average value and $f_i(\boldsymbol{X}^\star)$ denotes the global minimum of f_i.

Proof: Refer to Appendix D. ∎

Algorithm 3: Alternating DC Algorithm for Problem $\mathscr{P}$

Input: $\boldsymbol{\Theta}_{\mathrm{U}}^0$, $\boldsymbol{\Theta}_{\mathrm{D}}^0$, and predefined threshold $\epsilon > 0$.
Output: $\mathrm{MSE}^\star$.
for $t \leftarrow 1, 2, \ldots$ **do**
  Given $\boldsymbol{\Theta}_{\mathrm{U}}^{t-1}$ and $\boldsymbol{\Theta}_{\mathrm{D}}^{t-1}$, solve problem $\mathscr{P}_1$ to get $\boldsymbol{v}_{\mathrm{SDR}}^t$.
  if *The solution of problem* $\mathscr{P}_1$ *dose not satisfy the rank-one constraint* **then**
    Select an initial subgradient $\partial_{\boldsymbol{V}^0} \|\boldsymbol{V}\|_2$.
    Solve problem (31) by using Algorithm 2 to get $\boldsymbol{v}^t$.
  else
    $\boldsymbol{v}^t = \boldsymbol{v}_{\mathrm{SDR}}^t$.
  end
  Given $\boldsymbol{\Theta}_{\mathrm{D}}^{t-1}$ and $\boldsymbol{v}^t$, solve problem $\mathscr{P}_2$ to get $\boldsymbol{\Theta}_{\mathrm{U}}^t$.
  if *Problem* $\mathscr{P}_2$ *becomes infeasible* **then**
    Select an initial subgradient $\partial_{\boldsymbol{Z}^0} \|\boldsymbol{Z}\|_2$.
    Solve problem (32) by using Algorithm 2 to get $\boldsymbol{\Theta}_{\mathrm{U}}^t$.
  end
  Given $\boldsymbol{v}^t$ and $\boldsymbol{\Theta}_{\mathrm{U}}^t$, solve problem $\mathscr{P}_3$ to get $\boldsymbol{\Theta}_{\mathrm{D}}^t$.
  if *Problem* $\mathscr{P}_3$ *becomes infeasible* **then**
    Select an initial subgradient $\partial_{\boldsymbol{Q}^0} \|\boldsymbol{Q}\|_2$.
    Solve problem (33) by using Algorithm 2 to get $\boldsymbol{\Theta}_{\mathrm{D}}^t$.
  end
  if $\left|\mathrm{MSE}^t - \mathrm{MSE}^{t-1}\right| < \epsilon$ **then**
    $\mathrm{MSE}^\star = \mathrm{MSE}^t$.
    break.
  end
end

V. Numerical Results

In this section, we present the numerical results of the proposed alternating DC algorithm for the IRS-aided IoT networks. In the simulations, we consider a 3-D network, where the AP and the IRS are located at $(0, 0, 0)$ and $(20, 20, 0)$ m, respectively. In addition, the IoT devices are randomly distributed in the region of $([20, 60], [-20, 20], 0)$ m. As in [37] and [38], we consider large-scale path loss and small-scale Rayleigh fading. The path-loss exponents of the links between the AP and the IoT devices, between the AP and the IRS, and between the IRS and the IoT devices are set to be 3.5, 2.2, and 2.3, respectively, similar to [24] and [34]–[36]. We assume that the maximum transmit power at the AP is $P_{\max} = 1000$ mW and the power of AWGN is -60 dBm. The effective power conversion efficiency $\mu_k \alpha_k \ \forall k$, follows a uniform distribution within the range of $(0, 1)$. The time duration ratio between the downlink EB phase and the uplink AirComp phase is set to be $T_{\mathrm{EB}}/T_{\mathrm{AC}} = 100$. The convergence thresholds ϵ_{DC} and ϵ are set to be 10^{-5} and 10^{-4}, respectively.

To reduce the computation complexity, we first utilize the SDR method to solve problem $\mathscr{P}_1$. If the returned solution does not meet the rank-one constraint, then the DC algorithm is applied. Besides, we do not use the DC method to find the feasible solutions of problems (18) and (21) until problems $\mathscr{P}_2$ and $\mathscr{P}_3$ solved by the SDR method become infeasible. As a result, the computation complexity of Algorithm 3 is reduced. Meanwhile, Algorithm 3 outperforms Algorithm 1 in terms of minimizing MSE, as shown in the following results.

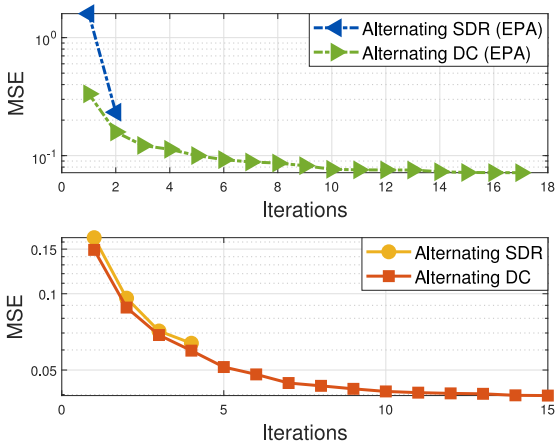

Fig. 3. MSE versus the number of iterations when $K = 20$, $M = 30$, and $N = 40$.

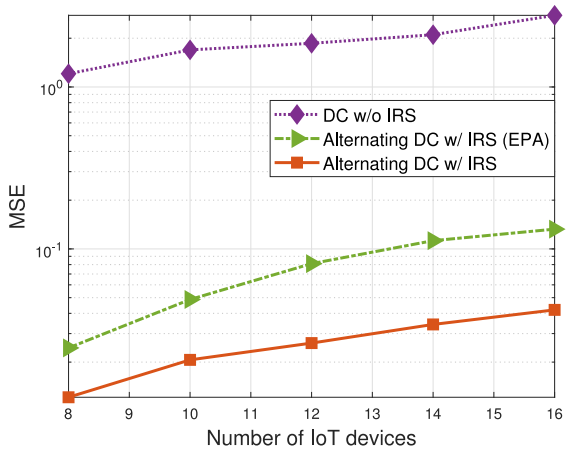

Fig. 4. MSE versus the number of IoT devices when $M = 30$ and $N = 40$.

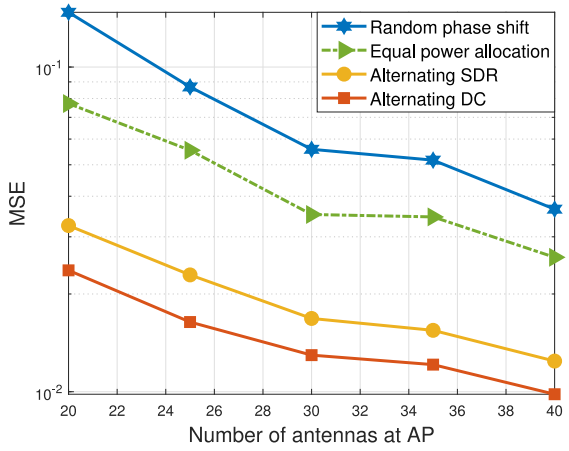

Fig. 5. MSE versus the number of antennas at the AP when $K = 15$ and $N = 40$.

We consider two baseline methods, i.e., equal power allocation (EPA) and random phase shift. For EPA, the AP allocates the same transmit power $P_k = P_{\max}/K$ to wirelessly power each IoT device and we solve the resulting optimization problem by using either the alternating SDR algorithm summarized in Algorithm 1 or the alternating DC algorithm summarized in Algorithm 3. By comparing with the EPA scheme, the importance of optimizing the EB vector in the downlink EB phase is better illustrated. For the random phase shift method, we first choose fixed random phase-shift matrices $\mathbf{\Theta}_{\mathrm{D}}$ and $\mathbf{\Theta}_{\mathrm{U}}$, and then solve problem $\mathscr{P}_1$.

Fig. 3 shows the convergence behaviors of the alternating SDR and DC algorithms as well as their simplified versions with EPA when $K = 20$, $M = 30$, and $N = 40$. It can be observed that the alternating SDR algorithm terminates the iteration earlier than the alternating DC algorithm. This is because the alternating SDR algorithm fails to find a feasible solution after a few iterations, even after utilizing the Gaussian randomization technique for problem $\mathscr{P}_2$ or $\mathscr{P}_3$. In contrary, the alternating DC algorithm guarantees to find the rank-one solutions of problems $\mathscr{P}_1$, $\mathscr{P}_2$, and $\mathscr{P}_3$. In addition, the alternating DC algorithm achieves a lower MSE than the alternating SDR algorithm, as dropping the rank-one constraints leads to the performance degradation of the SDR algorithm. Furthermore, we can also observe that the proposed algorithm achieves a better MSE performance than the EPA method, which demonstrates the importance of jointly optimizing the phase shifts and the EB vectors.

Fig. 4 shows the MSE of different algorithms versus the number of IoT devices for IoT networks with and without an IRS when $M = 30$ and $N = 40$. Compared to the scenario without an IRS, deploying an IRS in IoT networks can significantly reduce the MSE of AirComp, which validates the effectiveness of deploying an IRS. In addition, as the number of IoT devices increases, the MSE of all methods increases, indicating that there exists a tradeoff between the quantity and the quality of WDA. Compared to the EPA method, the proposed alternating DC algorithm optimizes the downlink EB vectors to improve the energy harvested by IoT devices, which in turn yields a lower MSE.

Fig. 5 illustrates the impact of the number of antennas at the AP on the MSE when $K = 15$ and $N = 40$. As the number of antennas at the AP increases, the power gains achieved by both the IoT devices in the downlink and the AP in the uplink increase, which in turn reduce the MSE. In addition, it is observed that the proposed alternating DC algorithm and the alternating SDR algorithm both achieve much better performance than the random phase shift and EPA baseline methods, which demonstrates the importance of jointly optimizing the phase shifts and the aggregation beamforming vectors. Moreover, by inducing the exact rank-one solutions, the proposed alternating DC algorithm achieves lower AirComp distortion than the alternating SDR algorithm with Gaussian randomization.

Fig. 6 shows the impact of the number of passive reflecting elements at the IRS on the MSE when $K = 15$ and $M = 30$. As the number of elements at the IRS increases, the MSE of all methods decreases significantly, which indicates that having more passive reflecting elements leads to better performance. This is due to the fact that the IRS having more elements is capable of generating more accurate reflective beamforming for the incident signals. Furthermore, the proposed alternating DC algorithm outperforms all the baseline methods for different number of elements at the IRS.

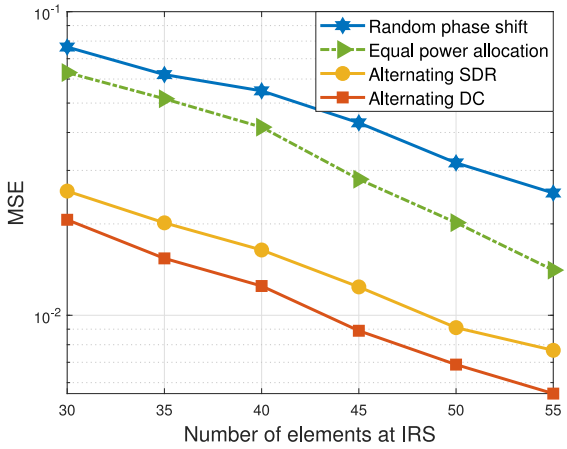

Fig. 6. MSE versus the number of elements at the IRS when $K = 15$ and $M = 30$.

VI. Conclusion

In this article, we leveraged the IRS to enhance the performance of wireless-powered data aggregation via AirComp in IoT networks. We formulated an MSE minimization problem to jointly optimize the energy and aggregation beamformers at the AP, the downlink/uplink phase-shift matrices at the IRS, as well as the transmit power at the IoT devices. We developed an alternating minimization method to decouple the downlink EB and uplink AirComp, yielding alternating SDP problems. We reformulated rank-one constrained matrix optimization problems as DC programming problems, followed by proposing an effective alternating DC algorithm to obtain the optimal rank-one solution via successively solving the primal and dual problems of DC functions. Simulations demonstrated the effectiveness of deploying an IRS in boosting the performance of wireless-powered AirComp in IoT networks and showed that the proposed algorithm outperforms the baseline methods. For future works, we will extend this work to consider discrete phase shifts at the IRS and optimize the time duration ratio between the downlink EB and uplink AirComp phases. In addition, we will further develop a scalable algorithm based on the first-order optimization method, such as the alternating direction method of multipliers (ADMMs) [51], to facilitate large-scale optimization in IRS-aided IoT networks.

Appendix A
Proof of Lemma 1

It is obvious that both the first and the second terms in (9a), i.e., $\sum_{k=1}^{K} |(1/\sqrt{\eta})\boldsymbol{v}^{\mathsf{H}}\boldsymbol{f}_{\mathrm{U},k}\beta_k - 1|^2$ and $\sigma^2\|\boldsymbol{v}\|^2/\eta$, are positive. Therefore, we have

$$\sum_{k=1}^{K}\left|\frac{1}{\sqrt{\eta}}\boldsymbol{v}^{\mathsf{H}}\boldsymbol{f}_{\mathrm{U},k}\beta_k - 1\right|^2 + \frac{\sigma^2\|\boldsymbol{v}\|^2}{\eta} \geq \frac{\sigma^2\|\boldsymbol{v}\|^2}{\eta} \tag{55}$$

and the equality holds when

$$\sum_{k=1}^{K}\left|\frac{1}{\sqrt{\eta}}\boldsymbol{v}^{\mathsf{H}}\boldsymbol{f}_{\mathrm{U},k}\beta_k - 1\right|^2 = 0. \tag{56}$$

Based on (56), we obtain $\beta_k^\star$ as in (10).

In addition, as each transmit scalar β_k needs to satisfy the power constraint (9b), we have

$$|\beta_k^\star|^2 = \frac{\eta}{\left|\boldsymbol{v}^{\mathsf{H}}\boldsymbol{f}_{\mathrm{U},k}\right|^2} \leq \zeta_k\left|\boldsymbol{f}_{\mathrm{D},k}\boldsymbol{\omega}_k\right|^2 \quad \forall k \in \mathcal{K}. \tag{57}$$

Thus, η should be equal to $\min_k\ \zeta_k|\boldsymbol{f}_{\mathrm{D},k}\boldsymbol{\omega}_k|^2|\boldsymbol{v}^{\mathsf{H}}\boldsymbol{f}_{\mathrm{U},k}|^2$.

Appendix B
Proof of Proposition 1

By assuming $\tau = \min\limits_k\ \zeta_k P_k\|\boldsymbol{f}_{\mathrm{D},k}\|^2|\boldsymbol{v}^{\mathsf{H}}\boldsymbol{f}_{\mathrm{U},k}|^2$, problem (14) is equivalent to the following optimization problem:

$$\begin{aligned}\underset{\boldsymbol{\Theta}_{\mathrm{D}},\boldsymbol{v},\boldsymbol{\Theta}_{\mathrm{U}},\{P_k\}}{\text{minimize}}\quad & \|\boldsymbol{v}\|^2/\tau \\ \text{subject to}\quad & \zeta_k P_k\|\boldsymbol{f}_{\mathrm{D},k}\|^2|\boldsymbol{v}^{\mathsf{H}}\boldsymbol{f}_{\mathrm{U},k}|^2 \geq \tau \quad \forall k \in \mathcal{K} \\ & \text{constraints (9d), (9e), (14b).}\end{aligned} \tag{58}$$

By further introducing a new optimization variable $\tilde{\boldsymbol{v}} = \boldsymbol{v}/\sqrt{\tau}$, the above problem can be rewritten as

$$\begin{aligned}\underset{\boldsymbol{\Theta}_{\mathrm{D}},\tilde{\boldsymbol{v}},\boldsymbol{\Theta}_{\mathrm{U}},\{P_k\}}{\text{minimize}}\quad & \|\tilde{\boldsymbol{v}}\|^2 \\ \text{subject to}\quad & \zeta_k P_k\|\boldsymbol{f}_{\mathrm{D},k}\|^2|\tilde{\boldsymbol{v}}^{\mathsf{H}}\boldsymbol{f}_{\mathrm{U},k}|^2 \geq 1 \quad \forall k \in \mathcal{K} \\ & \text{constraints (9d), (9e), (14b),}\end{aligned} \tag{59}$$

which is the same as problem (15).

Appendix C
Proof of Proposition 3

The subgradient of the orthogonally invariant norm $\|\boldsymbol{X}\|_2$ of the PSD matrix $\boldsymbol{X}$ can be computed by [52]

$$\begin{aligned}\partial\|\boldsymbol{X}\|_2 = \mathrm{conv}\Big\{&\boldsymbol{U}\mathrm{diag}(\boldsymbol{d})\boldsymbol{U}^{\mathsf{H}}|\boldsymbol{X} = \boldsymbol{U}\boldsymbol{\Sigma}\boldsymbol{U}^{\mathsf{H}} \\ &\boldsymbol{d} \in \partial\|\boldsymbol{\sigma}(\boldsymbol{X})\|_\infty\}\end{aligned} \tag{60}$$

where $\mathrm{conv}\{\cdot\}$ denotes the convex hull of a set, and

$$\partial\|\boldsymbol{\sigma}(\boldsymbol{X})\|_\infty = \mathrm{conv}\{\boldsymbol{e}_i, i{:}\sigma_i(\boldsymbol{X}) = \sigma_1(\boldsymbol{X})\}. \tag{61}$$

As $\sigma_1(\boldsymbol{X}) \geq \sigma_2(\boldsymbol{X}) \geq \cdots \geq \sigma_m(\boldsymbol{X})$, we have

$$\boldsymbol{e}_1 = \left[\underbrace{1, 0, \ldots, 0}_{m}\right]^{\mathsf{T}} \in \partial\|\boldsymbol{\sigma}(\boldsymbol{X})\|_\infty \tag{62}$$

and therefore, the subgradient of $\|\boldsymbol{X}\|_2$ can be computed by $\boldsymbol{u}_1\boldsymbol{u}_1^{\mathsf{H}}$.

Appendix D
Proof of Proposition 4

We denote the sequence of dual variables as $\{\boldsymbol{Y}^t\}$, which corresponds to the sequence $\{\boldsymbol{X}^t\}$ constructed by iteratively solving convex subproblem (49). Due to the strong convexity of h_i, we have

$$h_i\left(\boldsymbol{X}^{t+1}\right) \geq h_i\left(\boldsymbol{X}^t\right) + \left\langle\Delta_t\boldsymbol{X}, \boldsymbol{Y}^t\right\rangle + \frac{\gamma}{2}\|\Delta_t\boldsymbol{X}\|_{\mathrm{F}}^2 \tag{63}$$

$$\left\langle\boldsymbol{X}^t, \boldsymbol{Y}^t\right\rangle = h_i\left(\boldsymbol{X}^t\right) + h_i^*\left(\boldsymbol{Y}^t\right) \tag{64}$$

where $\Delta_t \boldsymbol{X} = \boldsymbol{X}^{t+1} - \boldsymbol{X}^t$. By adding $g_i(\boldsymbol{X}^{t+1})$ to both sides of (63), we have

$$f_i\left(\boldsymbol{X}^{t+1}\right) \leq g_i\left(\boldsymbol{X}^{t+1}\right) - h_i\left(\boldsymbol{X}^t\right) - \left\langle \Delta_t \boldsymbol{X}, \boldsymbol{Y}^t \right\rangle - \frac{\gamma}{2}\|\Delta_t \boldsymbol{X}\|_{\mathrm{F}}^2 \tag{65}$$

where $f_i(\boldsymbol{X}^{t+1}) = g_i(\boldsymbol{X}^{t+1}) - h_i(\boldsymbol{X}^{t+1})$. Besides, for the update of primal variable $\boldsymbol{X}$ according to (48), the dual variable can be denoted by $\boldsymbol{Y}^t \in \partial_{\boldsymbol{X}^{t+1}} g_i$. Hence, due to the strong convexity of g_i, we have

$$g_i\left(\boldsymbol{X}^t\right) \geq g_i\left(\boldsymbol{X}^{t+1}\right) + \left\langle -\Delta_t \boldsymbol{X}, \boldsymbol{Y}^t \right\rangle + \frac{\gamma}{2}\|\Delta_t \boldsymbol{X}\|_{\mathrm{F}}^2 \tag{66}$$

$$\left\langle \boldsymbol{X}^{t+1}, \boldsymbol{Y}^t \right\rangle = g_i\left(\boldsymbol{X}^{t+1}\right) + g_i^*\left(\boldsymbol{Y}^t\right). \tag{67}$$

By subtracting $h_i(\boldsymbol{X}^t)$ from both sides of (66), we have

$$f_i\left(\boldsymbol{X}^t\right) \geq g_i\left(\boldsymbol{X}^{t+1}\right) - h_i\left(\boldsymbol{X}^t\right) + \left\langle -\Delta_t \boldsymbol{X}, \boldsymbol{Y}^t \right\rangle + \frac{\gamma}{2}\|\Delta_t \boldsymbol{X}\|_{\mathrm{F}}^2. \tag{68}$$

Moreover, by subtracting (67) from (64), we have

$$f_i^*\left(\boldsymbol{Y}^t\right) = g_i\left(\boldsymbol{X}^{t+1}\right) - h_i\left(\boldsymbol{X}^t\right) - \left\langle \Delta_t \boldsymbol{X}, \boldsymbol{Y}^t \right\rangle \tag{69}$$

where $f_i^*(\boldsymbol{Y}^t) = h_i^*(\boldsymbol{Y}^t) - g_i^*(\boldsymbol{Y}^t)$. After combining (65), (68), and (69), we have

$$\begin{aligned} f_i\left(\boldsymbol{X}^t\right) &\geq f_i^*\left(\boldsymbol{Y}^t\right) + \frac{\gamma}{2}\|\Delta_t \boldsymbol{X}\|_{\mathrm{F}}^2 \\ &\geq f_i\left(\boldsymbol{X}^{t+1}\right) + \gamma\|\Delta_t \boldsymbol{X}\|_{\mathrm{F}}^2 \end{aligned} \tag{70}$$

which implies that the sequence $\{f_i(\boldsymbol{X}^t)\}$ is nonincreasing. Furthermore, since $f_i \geq 0$ always holds, it can be concluded that the sequence $\{f_i(\boldsymbol{X}^t)\}$ is strictly decreasing until convergence, that is

$$\lim_{t\to\infty} \quad \|\Delta_t \boldsymbol{X}\|_{\mathrm{F}}^2 = 0. \tag{71}$$

When the sequence $\{f_i(\boldsymbol{X}^t)\}$ converges to a limit point at iteration t°, we have

$$\|\Delta_t \boldsymbol{X}\|_{\mathrm{F}}^2 = 0, \quad t \in \left\{t^\circ, t^\circ + 1, \ldots, \right\}. \tag{72}$$

Thus, according to (70), we also have

$$f_i\left(\boldsymbol{X}^t\right) = f_i^*\left(\boldsymbol{Y}^t\right) = f_i\left(\boldsymbol{X}^{t+1}\right). \tag{73}$$

Based on $f_i(\boldsymbol{X}^{t+1}) = g_i(\boldsymbol{X}^{t+1}) - h_i(\boldsymbol{X}^{t+1})$ and $f_i^*(\boldsymbol{Y}^t) = h_i^*(\boldsymbol{Y}^t) - g_i^*(\boldsymbol{Y}^t)$, we have

$$h_i\left(\boldsymbol{X}^{t+1}\right) + h_i^*\left(\boldsymbol{Y}^t\right) = g_i\left(\boldsymbol{X}^{t+1}\right) + g_i^*\left(\boldsymbol{Y}^t\right) = < \boldsymbol{X}^{t+1}, \boldsymbol{Y}^t > \tag{74}$$

which is equivalent to

$$\boldsymbol{Y}^t \in \partial_{\boldsymbol{X}^{t+1}} g_i \cap \partial_{\boldsymbol{X}^{t+1}} h_i \tag{75}$$

and it is concluded that $\boldsymbol{X}^{t+1}$ is a critical point of f_i.

Based on (70), the average value of sequence $\{\|\Delta_t \boldsymbol{X}\|_{\mathrm{F}}^2\}$ is given by

$$\begin{aligned} \mathbb{A}\left[\left\{\|\Delta_t \boldsymbol{X}\|_{\mathrm{F}}^2\right\}_{r=0}^{t}\right] &\leq \sum_{r=0}^{t} \frac{f_i\left(\boldsymbol{X}^t\right) - f_i\left(\boldsymbol{X}^{t+1}\right)}{\gamma(t+1)} \\ &\leq \frac{f_i\left(\boldsymbol{X}^0\right) - f_i\left(\boldsymbol{X}^{t+1}\right)}{\gamma(t+1)} \\ &\leq \frac{f_i\left(\boldsymbol{X}^0\right) - f_i\left(\boldsymbol{X}^\star\right)}{\gamma(t+1)} \end{aligned} \tag{76}$$

where $f_i(\boldsymbol{X}^\star)$ denotes the global minimum of f_i.

REFERENCES

[1] T. Taleb and A. Kunz, "Machine type communications in 3GPP networks: Potential, challenges, and solutions," *IEEE Commun. Mag.*, vol. 50, no. 3, pp. 178–184, Mar. 2012.

[2] L. Chettri and R. Bera, "A comprehensive survey on Internet of Things (IoT) toward 5G wireless systems," *IEEE Internet Things J.*, vol. 7, no. 1, pp. 16–32, Jan. 2020.

[3] K. B. Letaief, W. Chen, Y. Shi, J. Zhang, and Y.-J. A. Zhang, "The roadmap to 6G–AI empowered wireless networks," *IEEE Commun. Mag.*, vol. 57, no. 8, pp. 84–90, Aug. 2019.

[4] B. Nazer and M. Gastpar, "Computation over multiple-access channels," *IEEE Trans. Inf. Theory*, vol. 53, no. 10, pp. 3498–3516, Oct. 2007.

[5] O. Abari, H. Rahul, and D. Katabi. (2016). *Over-the-Air Function Computation in Sensor Networks*. [Online]. Available: http://arxiv.org/abs/1612.02307

[6] M. Goldenbaum and S. Stanczak, "Robust analog function computation via wireless multiple-access channels," *IEEE Trans. Commun.*, vol. 61, no. 9, pp. 3863–3877, Sep. 2013.

[7] L. Chen, X. Qin, and G. Wei, "A uniform-forcing transceiver design for over-the-air function computation," *IEEE Wireless Commun. Lett.*, vol. 7, no. 6, pp. 942–945, Dec. 2018.

[8] G. Zhu and K. Huang, "MIMO over-the-air computation for high-mobility multi-modal sensing," *IEEE Internet Things J.*, vol. 6, no. 4, pp. 6089–6103, Aug. 2019.

[9] L. Chen, N. Zhao, Y. Chen, F. R. Yu, and G. Wei, "Over-the-air computation for IoT networks: Computing multiple functions with antenna arrays," *IEEE Internet Things J.*, vol. 5, no. 6, pp. 5296–5306, Dec. 2018.

[10] J. Dong, Y. Shi, and Z. Ding, "Blind over-the-air computation and data fusion via provable wirtinger flow," *IEEE Trans. Signal Process.*, vol. 68, pp. 1136–1151, Jan. 2020.

[11] K. Yang, T. Jiang, Y. Shi, and Z. Ding, "Federated learning via over-the-air computation," *IEEE Trans. Wireless Commun.*, vol. 19, no. 3, pp. 2022–2035, Mar. 2020.

[12] K. Yang, Y. Shi, Y. Zhou, Z. Yang, L. Fu, and W. Chen, "Federated machine learning for intelligent IoT via reconfigurable intelligent surface," *IEEE Netw.*, 2020, doi: 10.1109/MNET.011.2000045.

[13] Z. Yang, M. Chen, W. Saad, C. S. Hong, and M. Shikh-Bahaei. (2019). *Energy Efficient Federated Learning Over Wireless Communication Networks*. [Online]. Available: http://arxiv.org/abs/1911.02417

[14] M. Chen, Z. Yang, W. Saad, C. Yin, H. V. Poor, and S. Cui. (2019). *A Joint Learning and Communications Framework for Federated Learning Over Wireless Networks*. [Online]. Available: http://arxiv.org/abs/1909.07972

[15] G. Zhu, Y. Du, D. Gunduz, and K. Huang. (2019). *One-Bit Over-the-Air Aggregation for Communication-Efficient Federated Edge Learning: Design and Convergence Analysis*. [Online]. Available: http://arxiv.org/abs/2001.05713

[16] M. Goldenbaum, H. Boche, and S. Stańczak, "Nomographic functions: Efficient computation in clustered Gaussian sensor networks," *IEEE Trans. Wireless Commun.*, vol. 14, no. 4, pp. 2093–2105, Apr. 2015.

[17] W. Liu, X. Zang, Y. Li, and B. Vucetic, "Over-the-air computation systems: Optimization, analysis and scaling laws," *IEEE Trans. Wireless Commun.*, vol. 19, no. 8, pp. 5488–5502, Aug. 2020.

[18] J. Zheng, Y. Cai, X. Shen, Z. Zheng, and W. Yang, "Green energy optimization in energy harvesting wireless sensor networks," *IEEE Commun. Mag.*, vol. 53, no. 11, pp. 150–157, Nov. 2015.

[19] Y. Wu, X. Yang, L. P. Qian, H. Zhou, X. Shen, and M. K. Awad, "Optimal dual-connectivity traffic offloading in energy-harvesting small-cell networks," *IEEE Trans. Green Commun. Netw.*, vol. 2, no. 4, pp. 1041–1058, Apr. 2018.

[20] Z. Hou, H. Chen, Y. Li, and B. Vucetic, "Incentive mechanism design for wireless energy harvesting-based Internet of Things," *IEEE Internet Things J.*, vol. 5, no. 4, pp. 2620–2632, Aug. 2018.

[21] X. Li, G. Zhu, Y. Gong, and K. Huang, "Wirelessly powered data aggregation for IoT via over-the-air function computation: Beamforming and power control," *IEEE Trans. Wireless Commun.*, vol. 18, no. 7, pp. 3437–3452, Jul. 2019.

[22] C. Huang *et al.* (2019). *Holographic MIMO Surfaces For 6G Wireless Networks: Opportunities, Challenges, and Trends*. [Online]. Available: http://arxiv.org/abs/1911.12296

[23] Q. Wu and R. Zhang, "Towards smart and reconfigurable environment: Intelligent reflecting surface aided wireless network," *IEEE Commun. Mag.*, vol. 58, no. 1, pp. 106–112, Jan. 2020.

[24] Q. Wu and R. Zhang, "Intelligent reflecting surface enhanced wireless network via joint active and passive beamforming," *IEEE Trans. Wireless Commun.*, vol. 18, no. 11, pp. 5394–5409, Nov. 2019.

[25] Y. Alsaba, S. K. A. Rahim, and C. Y. Leow, "Beamforming in wireless energy harvesting communications systems: A survey," *IEEE Commun. Surveys Tuts.*, vol. 20, no. 2, pp. 1329–1360, 2nd Quart., 2018.

[26] D. W. K. Ng, E. S. Lo, and R. Schober, "Wireless information and power transfer: Energy efficiency optimization in OFDMA systems," *IEEE Trans. Wireless Commun.*, vol. 12, no. 12, pp. 6352–6370, Dec. 2013.

[27] H. Ju and R. Zhang, "Throughput maximization in wireless powered communication networks," *IEEE Trans. Wireless Commun.*, vol. 13, no. 1, pp. 418–428, Jan. 2014.

[28] L. Liu, R. Zhang, and K.-C. Chua, "Multi-antenna wireless powered communication with energy beamforming," *IEEE Trans. Commun.*, vol. 62, no. 12, pp. 4349–4361, Dec. 2014.

[29] C.-F. Liu, M. Maso, S. Lakshminarayana, C.-H. Lee, and T. Q. Quek, "Simultaneous wireless information and power transfer under different CSI acquisition schemes," *IEEE Trans. Wireless Commun.*, vol. 14, no. 4, pp. 1911–1926, Apr. 2014.

[30] K. W. Choi, L. Ginting, P. A. Rosyady, A. A. Aziz, and D. I. Kim, "Wireless-powered sensor networks: How to realize," *IEEE Trans. Wireless Commun.*, vol. 16, no. 1, pp. 221–234, Jan. 2017.

[31] J. Xu, Z. Zhong, and B. Ai, "Wireless powered sensor networks: Collaborative energy beamforming considering sensing and circuit power consumption," *IEEE Wireless Commun. Lett.*, vol. 5, no. 4, pp. 344–347, Apr. 2016.

[32] Y. Yang, B. Zheng, S. Zhang, and R. Zhang, "Intelligent reflecting surface meets OFDM: Protocol design and rate maximization," *IEEE Trans. Commun.*, vol. 68, no. 7, pp. 4522–4535, Jul. 2020.

[33] S. Xia and Y. Shi, "Intelligent reflecting surface for massive device connectivity: Joint activity detection and channel estimation," in *Proc. IEEE ICASSP*, 2020, pp. 5175–5179.

[34] T. Jiang and Y. Shi, "Over-the-air computation via intelligent reflecting surfaces," in *Proc. IEEE Global Commun. Conf. (GLOBECOM)*, 2019, pp. 1–6.

[35] Q. Wu and R. Zhang, "Weighted sum power maximization for intelligent reflecting surface aided SWIPT," *IEEE Wireless Commun. Lett.*, vol. 9, no. 5, pp. 586–590, May 2019.

[36] X. Guan, Q. Wu, and R. Zhang. (2019). *Intelligent Reflecting Surface Assisted Secrecy Communication via Joint Beamforming and Jamming*. [Online]. Available: http://arxiv.org/abs/1907.12839

[37] C. Huang, A. Zappone, G. C. Alexandropoulos, M. Debbah, and C. Yuen, "Reconfigurable intelligent surfaces for energy efficiency in wireless communication," *IEEE Trans. Wireless Commun.*, vol. 18, no. 8, pp. 4157–4170, Aug. 2019.

[38] M. Fu, Y. Zhou, and Y. Shi. (2019). *Reconfigurable Intelligent Surface Empowered Downlink Non-Orthogonal Multiple Access*. [Online]. Available: http://arxiv.org/abs/1910.07361

[39] S. Hua, Y. Zhou, K. Yang, and Y. Shi. (2019). *Reconfigurable Intelligent Surface for Green Edge Inference*. [Online]. Available: http://arxiv.org/abs/1912.00820

[40] C. Huang, R. Mo, and C. Yuen, "Reconfigurable intelligent surface assisted multiuser MISO systems exploiting deep reinforcement learning," *IEEE J. Sel. Areas Commun.*, early access, Jun. 8, 2020. [Online]. Available: https://ieeexplore.ieee.org/document/9110869, doi: 10.1109/JSAC.2020.3000835.

[41] Z. Wang, L. Liu, and S. Cui. (2019). *Channel Estimation for Intelligent Reflecting Surface Assisted Multiuser Communications*. [Online]. Available: http://arxiv.org/abs/1911.03084

[42] X. Yuan, Y.-J. Zhang, Y. Shi, W. Yan, and H. Liu. (2020). *Reconfigurable-Intelligent-Surface Empowered 6G Wireless Communications: Challenges and Opportunities*. [Online]. Available: http://arxiv.org/abs/2001.00364

[43] O. Abari, H. Rahul, D. Katabi, and M. Pant, "Airshare: Distributed coherent transmission made seamless," in *Proc. IEEE Conf. Comput. Commun. (INFOCOM)*, Apr. 2015, pp. 1742–1750.

[44] Z. Luo, W. Ma, A. M. So, Y. Ye, and S. Zhang, "Semidefinite relaxation of quadratic optimization problems," *IEEE Signal Process. Mag.*, vol. 27, no. 3, pp. 20–34, May 2010.

[45] Z. Wang, Y. Shi, and Y. Zhou, "Wirelessly powered data aggregation via intelligent reflecting surface assisted over-the-air computation," in *Proc. IEEE VTC Spring*, Antwerp, Belgium, May 2020, pp. 1–5.

[46] M. Grant and S. Boyd. (Mar. 2014). *CVX: MATLAB Software for Disciplined Convex Programming, Version 2.1*. [Online]. Available: http://cvxr.com/cvx

[47] S. Boyd and L. Vandenberghe, *Convex Optimization*. Cambridge, U.K.: Cambridge Univ. Press, 2004.

[48] P. D. Tao and L. T. H. An, "Convex analysis approach to D.C. programming: Theory, algorithm and applications," *Acta Mathematica Vietnamica*, vol. 22, no. 1, pp. 289–355, Jan. 1997.

[49] R. T. Rockafellar, *Convex Analysis*, vol. 28. Princeton, NJ, USA: Princeton Univ. Press, 1970.

[50] P. Bouboulis, K. Slavakis, and S. Theodoridis, "Adaptive learning in complex reproducing kernel Hilbert spaces employing wirtinger's subgradients," *IEEE Trans. Neural Netw. Learn. Syst.*, vol. 23, no. 3, pp. 425–438, Mar. 2012.

[51] Y. Shi, J. Zhang, B. O'Donoghue, and K. B. Letaief, "Large-scale convex optimization for dense wireless cooperative networks," *IEEE Trans. Signal Process.*, vol. 63, no. 18, pp. 4729–4743, Sep. 2015.

[52] G. Watson, "Characterization of the subdifferential of some matrix norms," *Linear Algebra Appl.*, vol. 170, pp. 33–45, Jun. 1992.

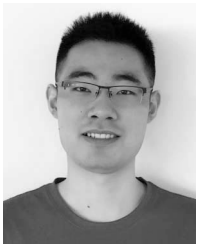

Zhibin Wang (Student Member, IEEE) received the B.S. degree in communication engineering from Xidian University, Xi'an, China, in 2019. He is currently pursuing the M.S. degree with the School of Information Science and Technology, ShanghaiTech University, Shanghai, China.

His research interests include Internet of Things networks and intelligent reflecting surface.

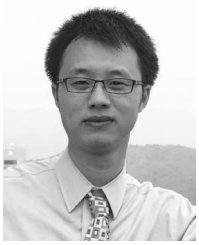

Yuanming Shi (Member, IEEE) received the B.S. degree in electronic engineering from Tsinghua University, Beijing, China, in 2011, and the Ph.D. degree in electronic and computer engineering from Hong Kong University of Science and Technology, Hong Kong, in 2015.

Since September 2015, he has been with the School of Information Science and Technology, ShanghaiTech University, Shanghai, China, where he is currently a tenured Associate Professor. He visited the University of California at Berkeley, Berkeley, CA, USA, from October 2016 to February 2017. His research areas include optimization, statistics, machine learning, signal processing, and their applications to 6G, IoT, and AI.

Dr. Shi was a recipient of the 2016 IEEE Marconi Prize Paper Award in Wireless Communications and the 2016 Young Author Best Paper Award by the IEEE Signal Processing Society. He is an Editor of the IEEE TRANSACTIONS ON WIRELESS COMMUNICATIONS.

Yong Zhou (Member, IEEE) received the B.S. and M.E. degrees from Shandong University, Jinan, China, in 2008 and 2011, respectively, and the Ph.D. degree from the University of Waterloo, Waterloo, ON, Canada, in 2015.

From November 2015 to January 2018, he worked as a Postdoctoral Research Fellow with the Department of Electrical and Computer Engineering, University of British Columbia, Vancouver, BC, Canada. He is currently an Assistant Professor with the School of Information Science and Technology, ShanghaiTech University, Shanghai, China. His research interests include Internet of Things, edge computing, and reconfigurable intelligent surface.

Haibo Zhou (Senior Member, IEEE) received the Ph.D. degree in information and communication engineering from Shanghai Jiao Tong University, Shanghai, China, in 2014.

From 2014 to 2017, he was a Postdoctoral Fellow with the Broadband Communications Research Group, Department of Electrical and Computer Engineering, University of Waterloo, Waterloo, ON, Canada. He is currently an Associate Professor with the School of Electronic Science and Engineering, Nanjing University, Nanjing, China. His research interests include resource management and protocol design in vehicular *ad hoc* networks, cognitive networks, and space–air–ground integrated networks.

Dr. Zhou was a recipient of the 2019 IEEE ComSoc Asia–Pacific Outstanding Young Researcher Award. He served as an Invited Track Co-Chair for ICCC'2019 and VTC-Fall'2020 and a TPC Member of many IEEE conferences, including GLOBECOM, ICC, and VTC. He served as an Associate Editor for the IEEE Comsoc Technically Co-Sponsored the *Journal of Communications and Information Networks* from April 2017 to March 2019, and a Guest Editor for the *IEEE Communications Magazine* in 2016, the *International Journal of Distributed Sensor Networks* (Hindawi) in 2017, and *IET Communications* in 2017. He is currently an Associate Editor of the IEEE INTERNET OF THINGS JOURNAL, *IEEE Network Magazine*, and IEEE WIRELESS COMMUNICATIONS LETTER.

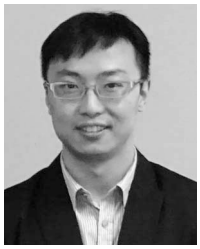

Ning Zhang (Senior Member, IEEE) received the Ph.D. degree in electrical and computer engineering from the University of Waterloo, Waterloo, ON, Canada, in 2015.

He was a Postdoctoral Research Fellow with the University of Waterloo and the University of Toronto, Toronto, ON, Canada, respectively. He is currently an Associate Professor with the University of Windsor, Windsor, ON, Canada. His research interests include vehicular and wireless networking, mobile-edge computing, and machine learning.

Dr. Zhang received the Best Paper Awards from IEEE Globecom in 2014, IEEE WCSP in 2015, IEEE ICC in 2019, IEEE ICCC in 2019, IEEE Technical Committee on Transmission Access and Optical Systems in 2019, and the *Journal of Communications and Information Networks* in 2018, respectively. He serves as an Associate Editor for the IEEE INTERNET OF THINGS JOURNAL, the IEEE TRANSACTIONS ON COGNITIVE COMMUNICATIONS AND NETWORKING, IEEE ACCESS, and *IET Communications*, and *Vehicular Communications* (Elsevier); and a Guest Editor of several international journals, such as IEEE WIRELESS COMMUNICATIONS, the IEEE TRANSACTIONS ON INDUSTRIAL INFORMATICS, and the IEEE TRANSACTIONS ON COGNITIVE COMMUNICATIONS AND NETWORKING. He also serves/served as a TPC Chair for IEEE SAGC 2020, a Track Chair for several international conferences, including IEEE VTC 2020, IEEE ICC 2022, AICON 2020, and CollaborateCom 2020, and a co-chair for numerous international workshops.